CDF/ANAL/TOP/CDFR/XXXX
Draft 0.0
February 15, 2013

Measurement of Single Top Production Cross Section in $\not\!\!E_T$ plus Jets Sample with the Full CDF Run II Data Set

Giorgio Bellettini, Marco Trovato
INFN Pisa, Italy

Fabrizio Margaroli
University of Rome 'La Sapienza', Italy

Karolos Potamianos
LBNL, USA

Daniela Bortoletto, Qiuguang Liu
Purdue University, USA

Matteo Cremonesi[1]
Oxford University, UK

Abstract

Top quarks are produced mostly in pairs at the Tevatron through the strong force. However, the electroweak force also allows the production of a single top quark with a cross section that is roughly half the $t\bar{t}$ one. In addition to the lower rate, the less distintinctive signature makes this process much harder to be separated from background. In the past, Tevatron experiments have always been looking for single top production in events where one high energy electron or muon is identified, as expected in the top leptonic decay channel $t \to Wb \to l\nu b$, in order to improve the signal signature over background. We present here a measurement of single top production cross section selecting events consistent with W+jets topology but where no electron or muon has been identifieded, and where the tau lepton in the $t \to Wb \to \tau\nu b$ channel is reconstructed as a jet in the calorimeters. Multivariate analysis techniques are necessary to suppress the large background and to discriminate the single top signal. We use the likelihood profile of this discriminant to estimate an expected production cross section $\sigma^{s+t}_{exp} = 3.20^{+1.39}_{-1.43}$ pb. In the CDF full data set we measure $\sigma^{s+t}_{obs} = 3.04^{+1.46}_{-1.39}$ pb.

[1]matteoc@fnal.gov

Contents

1 Introduction

The top quark has been studied extensively at the Tevatron since its discovery in 1995 [1] [2]. Because of its huge mass it can be expected to be specially sensitive to the mechanism by which particles acquire mass and, therefore, to have a special role in the process of electroweak symmetry breaking. Top has a lifetime shorter than the hadronization time, providing the unique opportunity to study a "nude" quark by analyzing its decay products.
In the Standard Model (SM), the top quark can be produced either via strong interaction as a $t\bar{t}$ pair or via electroweak interaction as a single top quark plus jets. Single top production was first observed by CDF and D0 in 2009 [3][4], 15 years after the discovery. Within the SM, the single-top signal allows for a direct measurement of the Cabibbo-Kobayashi-Maskawa(CKM) matrix element V_{tb}[5]. Furthermore, since the top quark decays before hadronization, its polarization can be directly observed in the angular correlations of its decay products[6][7]. Single top processes are expected to be sensitive to several kinds of new physics and CP violation.
At the Tevatron two single-top production modes are dominant (Fig. 1): the t-channel and the s-channel.

In t-channel production, a virtual space-like W boson strikes a b quark inside the

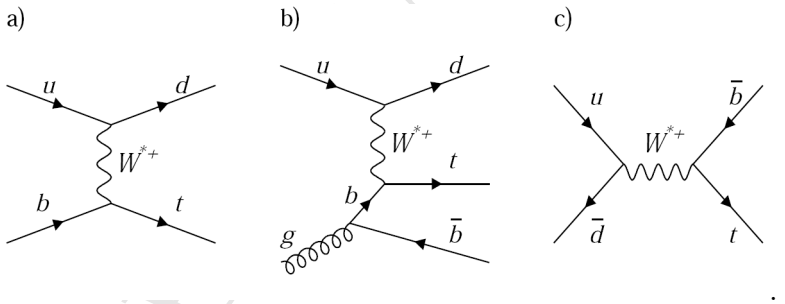

Figure 1: Feynman diagrams of dominant single-top production processes at the Tevatron: (a) t-channel at leading order (b) t-channel 2 3 process at NLO with initial state gluon splitting, (c) s-channel at leading order

proton or anti-proton. With a predicted cross-section of 2.10±0.19 pb at Tevatron, t-channel gives the largest contribution to the total number of single top events.

In the s-channel production, also referred to as W* production, a time-like W boson is produced by the quark-antiquark annihilation process. The predicted cross section of the s-channel at Tevatron is 1.05±0.07 pb.

At Tevatron Wt production mode, in which a top quark is produced in association with a real W boson, has a negligible cross section (0.22±0.08 pb)[8][9][10].

This note describes our measurement of electroweak single top quark production using the full $p\bar{p}$ collision data set collected in the CDF Run II up to the end of the Tevatron run in September 2011, corresponding to a total integrated luminosity of 9.1 fb^{-1}. The cross section being so small and the processes that mimic the signal so large, CDF and D0 have not been able to measure the cross section of this interesting process with full-prove significance. In order to increase the scanty statistics, we look here at events rejected by previous analyses, i.e. events where there are no identified leptons, or where τs are reconstructed as a jet. We thus rely solely on the signature of high P_T jets and large missing transverse energy. Being statistically independent of the lepton+jets sample, this sample provides, albeit with low precision, an independent measurement of the single top production cross section. Eventually, the result of this measurement can be combined with the lepton+jets one and help reaching a solid single top cross section measurement at the Tevatron.

2 Event Pre-Selection

Since we require large missing transverse energy and no leptons, we use a set of loose lepton identification cuts to make sure that we reject all events with true leptons. To impose track isolation we use a slightly modified version of the commonly used CMIO muon identification cuts [12]. We constructed these cuts to be loose enough to make sure that we exclude the single top signal already considered in the channel with identified leptons.

Jets are reconstructed off line using the JetClu algorithm with a cone in the $\eta - \phi$ space of radius R=0.4. We denote as "tight" jets with $|\eta| < 2.4$ and uncorrected transverse energy $E_T > 10$ GeV. We correct a jet four momentum appling the jet energy corrections up to level 5. We further correct jets by reconstructing their four-momenta according to the H1 prescription [13]. The H1 algorithm provides a slight increase in jet energy resolution. Tight jets are finally required to have H1-corrected $E_T > 15$ GeV. In this analysis we require $\not\!\!E_T > 50$ GeV and E_T $(j_1) > 35$ GeV, E_T $(j_2) > 25$ GeV. We then apply the trigger parameterization described in [24] to our Monte Carlo simulations. It was observed that the trigger efficiency depends also on the difference in R-space between the two jets. We preserve this choice which maintains the trigger fully efficient: $\Delta R > 1$ (to avoid cluster merging at L2, which would result in a loss of efficiency). The two leading jets are required to be not very forward: $|\eta|(j_i) < 2$, while the leading jet is required to be very central to match the trigger requirements $|\eta|(j_1) < 0.9$. We accept events with 2 or 3 tight jets. We expect events with mostly 2 jets in the s-channel, while single top appears as events with three jets in the NLO t-channel events, or where the charged lepton coming from the W is reconstructed as a jet[2]. In fact, in some cases the W decays to $e\nu$ and the electron fails the identification algorithm, but is reconstructed as a jet by JetClu; or when the W decays to $\tau\nu$ and $\tau \to$ hadrons. Finally, we accept events where one of the final state quarks radiates a quark or a gluon. We checked the acceptance to hadronic decays of the W from single top events, which resulted very small (less than 2%). As can be seen in Tables 1, 2, we have acceptance roughly half of the time to events where the W decays to τs the rest being split in electrons and muons. Since electrons and τs leave energy in the calorimeter, they can be reconstructed as jets by JetClu. As seen again in Tables 1, 2, this happens roughly 40% of the times (primarily due to taus).

s-channel	$W \to e\nu$	$W \to \mu\nu$	$W \to \tau\nu$
all events	19%	30%	51%
2 jet events	20%	34%	46%
3 jet events	17%	24%	59%

Table 1: Contributions to events with 2 or 3 jets from different leptonic decay modes of the W-boson in single top s-channel events

[2]Or whenever there is additional radiation from the initial or final state.

t-channel	$W \to e\nu$	$W \to \mu\nu$	$W \to \tau\nu$
all events	19%	29%	51%
2 jet events	21%	32%	47%
3 jet events	17%	23%	61%

Table 2: Contributions to events with 2 or 3 jets from different leptonic decay modes of the W-boson in single top t-channel events

In order to improve the signal-to-background ratio further, we need to identify jets originating from a b-quark. We do so employing both the SECVTX and JetProb b-tagging algorithms. We subdivide the sample into three orthogonal tagging categories (S stands for tight SECVTX tag, J stands for JetProb <5%):

- 1S: only one of the 2 leading jets is tagged by SecVTX
- SJ: one of the 2 leading jets is tagged by SecVTX, and the other one is not tagged by SecVTX but by JetProb
- SS: both of the leading jets are tagged by SecVTX.

Most background processes considered in this analysis produce real high $\not\!\!E_T$, e.g. W/Z decays to neutrinos or muons, which escape detection in the calorimeter. Additionally b-quarks produced in an event can decay semi-leptonically and produce real $\not\!\!E_T$. Mis-measurements in the calorimeter, on the other hand, can cause a QCD multijet event which has no real $\not\!\!E_T$ to appear with energy imbalance in the transverse plane. Since QCD multijet production has a very large cross-section, these events constitute a large fraction of $\not\!\!E_T$+jets data sample. With the relatively low $\not\!\!E_T$ cut and no leptons, most data at this analysis stage are composed of QCD production of two or three jets, where one of the jets is poorly measured, resulting in a large transverse energy imbalance. Due to this mismeasurement, most of the time the poorly measured jet will be the second highest E_T jet; the $\not\!\!E_T$ will as a consequence be aligned to it in the transverse plane. We label events having $\Delta\phi(\not\!\!E_T,\, j_2) < 0.4$ as our QCD control region; this events are used to derive a data-driven background modeling [14] and to check the same technique on a very pure QCD region. To define the signal region the above cut is reversed ($\Delta\phi(\not\!\!E_T,\, j_2) > 0.4$).

2.1 List of Preselection Cuts

We summarize the preselection cuts in the following list;

- lepton veto = use loose identification cuts to reject events with isolated leptons
- $\not\!\!E_T > 50$ GeV

- Number of jets = 2 or 3 and one of the leading jets (j1 or j2) central ($|\eta| < 0.9$). Events with a larger number of jets are rejected
- $\Delta R(j_1, j_2) > 1$
- $E_T(j_1) > 35$ GeV, $E_T(j_2) > 25$ GeV
- Events are b-tagged either 1S, SS, or SJ

	1S	SJ	SS
t-channel	197.3 ± 0.7	10.0 ± 0.1	10.9 ± 0.2
s-channel	113.9 ± 0.4	37.4 ± 0.2	45.0 ± 0.2
multijet	12630.3 ± 71.2	1044.6 ± 12.3	413.9 ± 9.4
wjet	3045.5 ± 21.3	96.3 ± 1.6	67.9 ± 1.3
zjet	1261.6 ± 3.8	46.9 ± 0.5	39.8 ± 0.5
diboson	277.2 ± 2.2	28.0 ± 0.5	26.9 ± 0.5
ttbar	965.2 ± 3.7	185.0 ± 1.4	202.5 ± 1.7
Expected	18490.9 ± 74.6	1448.3 ± 12.5	806.9 ± 9.7
Data	18494	1448	807

Table 3: Event yields after pre-selection cuts. Only statistical uncertainties are reported. Total expected events are forced to be equal to data at this stage by using fitted values for QCD multijet and V+jets rates (See Section 3.4.1).

3 Composition and Modeling of the Selected Data Sample

We analyze the full dataset collected by CDF in Run II up to period 38. The selected data sample corresponds to an integrated luminosity of about 9.1 fb^{-1}. We use the high-$\not\!\!E_T$ data stream (*emet*) accepting a combination of $MET35$, $MET45$ and MET_DIJET trigger paths. We estimate the expected composition of the selected sample in a sequence of steps by using a method which is similar to Method2, used in several analyses at CDF, which exploits heavy flavor tagging algorithms [17]. The method assumes that the following processes contribute to the selected data sample:

- Single Top and Diboson: our signal and and one of our background, diboson production, are both characterized by accurately **predicted** cross sections.
- top-antitop production: process characterized by accurately **measured** cross sections.
- QCD: multi-jet production whose normalization must be obtained from data.
- V+jets: production of a W/Z-boson associated to hadron jets whose normalization must be obtained as above.

The steps implemented by the method are the following:

- The contribution of processes whose cross sections are well known is estimated.
- The contribution of QCD and of W/Z+jets is estimated with a data-driven method (fit in QCDNN Sec. 3.4.1).

We avoid using the imprecise theoretical predictions for the production cross section of W/Z-boson with associated jets [18].

3.1 Signal Sample

To model the **single top** dynamics and predict both shape and rate, we use a sample generated with Powheg. The official sample is actually composed of three subsamples, one s-channel sample, a LO and a NLO t-channel sample.

3.2 Diboson MC Sample

We use the LO Pythia cross-sections scaled by a k-factor corresponding to the ratio between the NLO and LO cross-section prediction in MCFM[3] to predict both shape and rate of **diboson** production. The LO MCFM predictions are also consistent with

[3]MCFM stands for Monte Carlo for FeMtobarn

those from Pythia and are reported to be in good agreement with the data. To estimate the contribution of mistagged light flavor diboson events in the tag sample we apply the corresponding mistag matrix to diboson light flavor MC samples, vetoing events with a real b- or c-quark from HEPG. Details on the mistag rate matrix can be found in [15].

3.3 $t\bar{t}$ production

Top pair-production yields a significant contribution to the background in the pre-selection region, especially in the double-tag sample. Semi-leptonic top decays are energetic, bear large $\not\!\!E_T$ and high jet multiplicity. We use Monte Carlo samples generated for the Top Group to model the shape of this background. The $t\bar{t}$ events were generated with Pythia with $m_{top} = 172.5$ GeV and normalized with the cross section measured by CDF: 7.71±0.51 pb [16].

3.4 Multijet and V+jets backgrounds

V+jets background was generated with Alpgen+Pythia. As for diboson production, the contribution of mistagged light flavor V+jets events was determined by applying the mistag rate matrix to W/Z+lf samples vetoing events with a real b- or c-quark from HEPG.

The most significant background at the first stage of the analysis is the QCD multijet processes. QCD jet production has a large cross-section (several μb), which is about 6 orders of magnitude larger than the signal before requiring the first b-tag. Although, these processes generally do not have intrinsic $\not\!\!E_T$, mismeasured jets cause imbalance in the total transverse energy by which the QCD events can pass the basic selection cuts if one of the jets is also mis-tagged. Furthermore, QCD b-quark pair production yields taggable jets and if one b undergoes a semi-leptonic decay large $\not\!\!E_T$ can be generated. In both cases the missing transverse energy tends to be aligned parallel or anti-parallel to the first or second most energetic jet. This topology provides us one of the most effective tools for discriminating the QCD background. Due to the large cross-sections, it is practically impossible to generate enough statistics to simulate all QCD processes. To deal with this problem a method for estimating QCD background from data was developed [14]. This technique allows us to estimate not only heavy flavor QCD production, but also processes with a light flavor jet falsely tagged as a b-quark. Additionaly it allows us to model Single SecVTX tagged data sample, which adds additional sensitivity to the analysis.

3.4.1 Estimation of QCD and V+jets content - QCDNN fit

To reject a large part of multijet background, a Neural Network, referred as **QCDNN**, was trained. Details about the development of this multivariate object can be found in Section 4.1. Before cutting on the output of this NN, we use it to define the signal region, we fitted its distribution in order to estimate the normalization of both QCD and V+jets backgrounds. We choose this variable to perform the fit because the QCD background is well separated from the other electroweak processes and its normalization can be derived with a good precision. The fit is performed by using a **binned likelihood fit** (in particular, I used the TFractionFitter function in ROOT[4]). Four templates are used for the fit:

- **EW**: MC-based template built using EW selected events (single top, diboson). The normalization of this template is constrained to the theoretical predicted rate within its uncertainty (Section 3.2).
- $t\bar{t}$: The normalization of $t\bar{t}$ template is constrained to the measured cross section within its uncertainty (Section 3.3).
- **V+jets**: W/Z+jets selected events. The normalization of this template is a free parameter of the fit. As pre-fit rate we use the theoretical predicted rate.
- **QCD**: data-driven template. The normalization of this template is a free parameter of the fit. Since we do not have a theoretical predicted rate for this template, as pre-fit value we use the difference between data and the sum of the pre-fit predicted rates of all the others templates. In this way, the total expected number of events is forced to be equal to data.

The fit is performed indipendently in 1S, SJ and SS region. TFractionFitter returns the fraction of the total number of events fitted for every template, so it leaves the total expected number unchanged. For this reason the total expected number is going to be equal to data also post-fit. Using the percentages derived by the fit multiplied for the total expected number of events, we obtain the post-fit rates for V+jets and QCD. In Fig 2 post-fit distributions of the four templates are shown.

Template	Fraction 1S	Fraction SJ	Fraction SS
V+jets	0.2360 ± 0.0084	0,0994 ± 0.0331	0.1374 ± 0.0511
ewk	0.0350 ± 0.0012	0.0573 ± 0.0082	0.0924 ± 0.0125
multijet	0.6744 ± 0.0102	0.7081 ± 0.0407	0.5379 ± 0.0466
ttbar	0.0556 ± 0.0042	0.1362 ± 0.0124	0,2344 ± 0,0294

Table 4: Fitted fractions returned by TFractionFitter with their uncertainties.

[4] http://root.cern.ch/root/htmldoc/TFractionFitter.html

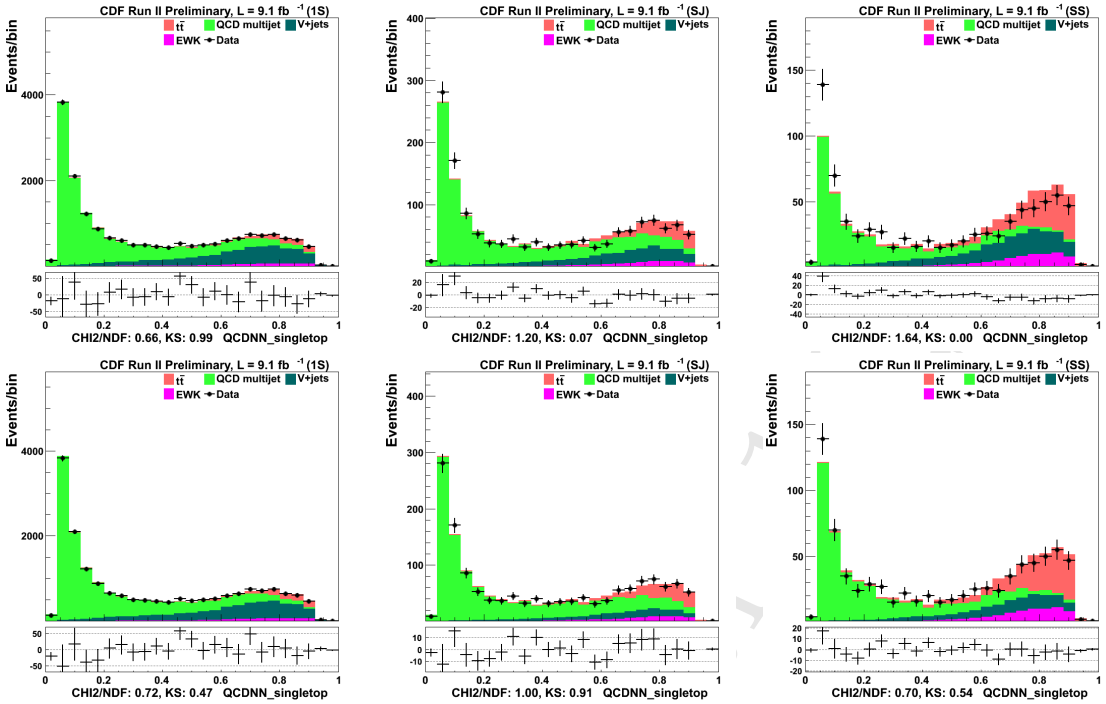

Figure 2: (Top) pre-fit and (Bottom) post-fit distributions of QCDNN in 1S, SJ, SS regions with subtraction plots.

4 Analysis Strategy

Having no identified leptons in the final state, backgrounds are many orders of magnitude larger than the signal even after requiring large missing transverse energy and b-tagged jets in the final state. It is thus necessary to develop an event selection which reduces backgrounds to a more manageable size before trying to build a discriminant to measure the single top cross section.

The **QCD multijet production** is the only background where the $\not\!\!E_T$ is mainly instrumental. In a first step we study the kinematics of these events and implement a multivariate technique to cut them out as much as possible.

We develop in a second step a discriminant to act against $t\bar{t}$ background. **Top pair production** gives a large contribution to total background, especially when both the leading jets in the final states are required to be b-tagged. In addition, the production of real top quarks makes this background more signal like if we take into account variables connected to the top mass, that are instead particularly useful in separating single top from all other non-top backgrounds. Following the prescriptions described in [11] and adapting them to the present analysis, we trained a neural network to reject $t\bar{t}$.

In the final step, we use again a machine learning technique to discriminate the

signal from the surviving backgrounds, and scan its output distribution to measure the single top production cross section in the $\not\!\!E_T$+jets final state.

4.1 Multijet Neural Network, QCDNN

The first step of our analysis strategy consists of training a Neural Network (NN) to reject multijet background as much as possible. As can be seen on Table 4 QCD is the largest contributor, amounting in the three tag samples from 50% to 70% of the total background . Developing a powerful QCD NN to remove multijet events is essential in order to reach a reasonable S/B ratio. We investigated the kinematics of the events, using the QCD plus mistags modeling derived from applying a tag rate parameterization to the data. Looking at a large set of variables, we keep those which have a very different behavior with respect to the signal. The single top signal used for the training is a mixture of 50% s-channel events and 50% t-channel events, which is roughly what we expect to be accepted after the event selection described in the previous paragraph. We use only events with at least one tight tag. The background is pre-tag data weighted by a tag rate parameterization function, which is a good approximation of the QCD multijet background. The multivariate technique used here is an artificial neural network (ANN or NN). We use a MultiLayerPerceptron (MLP) as implemented in the TMVA[5] package. Our network has 2 hidden layers. The nodes of each layer are 13:16:13:1. The neuron activation function is the hyperbolic tangent. We use a LearningRate of 0.01 and a TestRate of 5. The other parameters are set to the default in TMVA. We train for 500 epochs and check the convergence plots for overtraining. The 13 input variables are:

- missing transverse momentum, MPT
- missing transverse energy, $\not\!\!E_T$
- difference in ϕ between missing transverse energy $\not\!\!E_T$ and missing transverse momentum MPT, $\Delta\phi(\not\!\!E_T$, MPT)
- maximum difference in R-space between two jets, or all jet pairs
- minimum difference in ϕ between the $\not\!\!E_T$ and each jet
- minimum difference in ϕ between the MPT and the jets, considering all (MPT, j_i) pairings
- maximum difference in ϕ between jet directions, for all jet pairs;
- ratio of MHT (vector sum of tight jet ET) over $\not\!\!E_T$
- $\Delta\phi$ between the direction of the leading jets in jet pair rest frame and the direction of the jet pair boost

[5] http://tmva.sourceforge.net/

- $\not\!\!E_T$ /HT :HT being the scalar sum of the two leading jets E_T;
- $\not\!\!E_T$ significance : $\not\!\!E_T$ over the square root of sum E_T (over all calorimetric activity)
- invariant mass of $\not\!\!E_T$, j_1 and j_2
- Event sphericity : S = $1.5\times(\lambda_2 + \lambda_3)$, where λ_1 λ_2 and λ_3 are the second and third eigenvalues of the sphericity tensor.

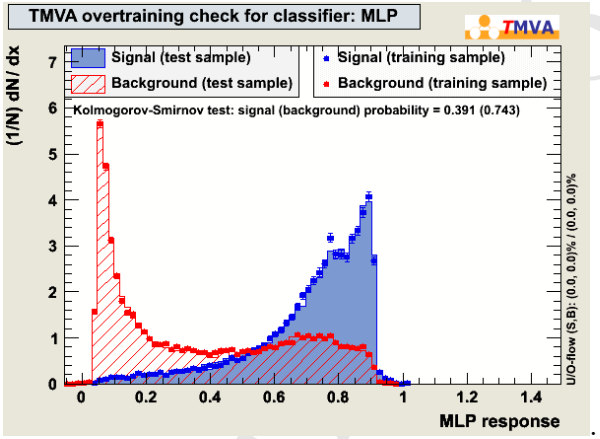

Figure 3: QCDNN output for the testing and training samples

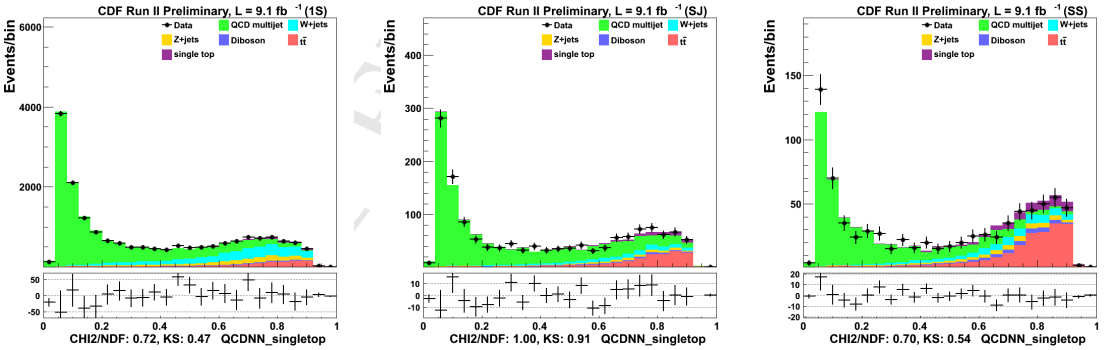

Figure 4: QCDNN stack plots in 1S, SJ, SS regions with subtraction plots on bottom.

Fig. 3 shows the NN output for the training and testing sample. Fig. 4 shows the stack plot of QCDNN with data, signal and backgrounds superimposed. It can be seen that this NN does a good job at discriminating multijet events, by moving most QCD background to the left, and most signal to the right of the distribution. We cut on this output at QCDNN > 0.35, to form the signal region. This cut removes almost 65% of the QCD multijet background, while keeping most of the signal (more than 90%).

	1S	SJ	SS
t-channel	185.8 ± 0.7	9.3 ± 0.1	10.2 ± 0.2
s-channel	106.2 ± 0.4	35.2 ± 0.2	42.8 ± 0.2
multijet	2878.4 ± 49.3	317.8 ± 8.9	92.5 ± 5.6
wjet	2647.9 ± 19.3	84.9 ± 1.5	61.3 ± 1.2
zjet	1111.0 ± 3.5	41.5 ± 0.4	35.7 ± 0.5
diboson	255.6 ± 2.1	26.0 ± 0.4	25.6 ± 0.5
ttbar	897.7 ± 3.6	172.8 ± 1.4	191.9 ± 1.6
Expected	8082.7 ± 53.2	687.4 ± 9.2	460.0 ± 6.0
Data	8222	704	448

Table 5: Event yields after QCDNN>0.35 cut. Only statistical uncertainties are reported

4.2 $t\bar{t}$ Neural Network, TTNN

The QCDNN mentioned above does a good job in separating the QCD events and the mistags. We are now going to address another major background: top pair production. Top-antitop background is one of the largest after the QCDNN cut and it is the more signal-like. With the same strategy adopted in the training of QCDNN, we look at a large set of variables, keeping only those in which $t\bar{t}$ events have a very different behavior with respect to the signal. Using only events with at least one tight tag, we built the signal template making a mixture of 50% s-channel events and 50% t-channel MC single top events. The background is simply $t\bar{t}$ MC. The nodes of each layer are 12:15:12:1. The neuron activation function is the hyperbolic tangent. We use a LearningRate of 0.01 and a TestRate of 5. The other parameters are set to the default in TMVA. We train for 500 epochs. The 12 input variables are:

- HT, the scalar sum of the two leading jets E_T and the $\not\!\!E_T$
- Vectorial sum of the jet pt
- Invariant transverse mass of $\not\!\!E_T$ and the 2 leading jets
- Invariant mass of j_1, j_2 and j_3
- Pt of the first jet
- Aplanarity
- Number of jets in the final state
- Missing Pt
- mht, vector sum of tight jet E_T
- Maximum difference in ϕ between two jets directions, over all jet pairs

- Pt of the second jet
- $\not\!\!E_T$, missing transverse energy

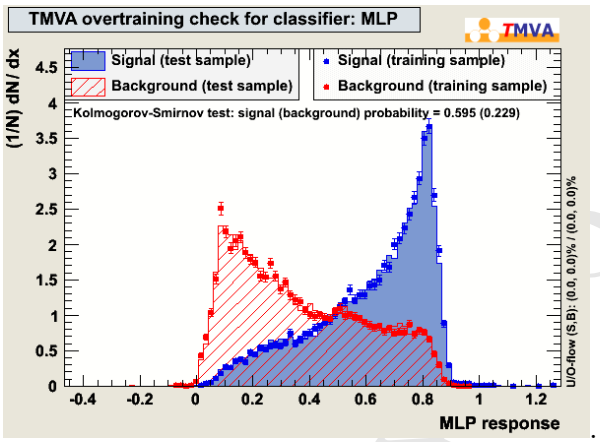

Figure 5: TTNN output for the testing and training samples

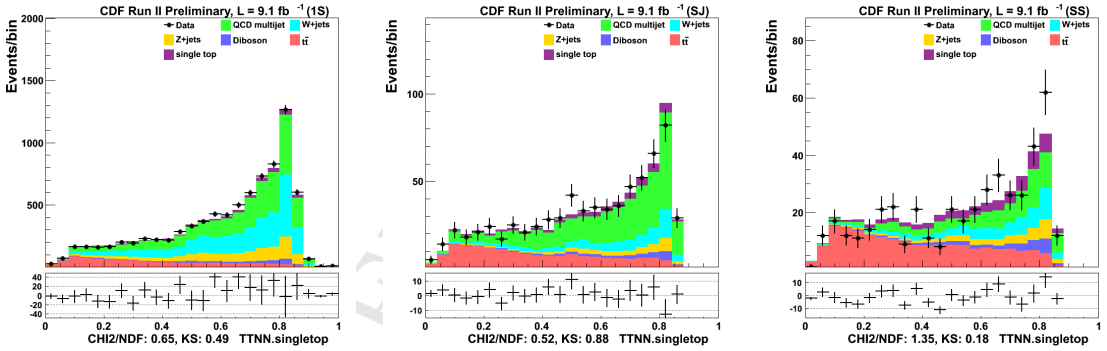

Figure 6: TTNN stack plots in 1S, SJ, SS regions with subtraction plots on bottom.

Fig. 5 shows the NN output for the training and testing sample. Fig. 6 shows the stack plot of TTNN with data, signal and backgrounds superimposed. We cut on this output at TTNN > 0.3, to form the signal region.With this cut almost 50% of $t\bar{t}$ background is removed, while keeping most of the signal events that passed the QCDNN cut (more than 90%).

4.3 Final Discriminant, SIGNN

The cuts on QCDNN and TTNN defined the signal region. We are now going to develop another NN as final discriminant between signal and the remaining background, that is going to be a mixture of top pair, W+h.f., Z+h.f and multijet. The single top signal used for the training is again a mixture of 50% s-channel events and 50% t-channel

	1S	SJ	SS
t-channel	170.0 ± 0.6	8.1 ± 0.1	8.8 ± 0.1
s-channel	94.1 ± 0.3	31.4 ± 0.2	38.4 ± 0.2
multijet	2642.1 ± 47.7	284.0 ± 8.7	85.9 ± 5.5
wjet	2425.1 ± 19.0	77.0 ± 1.4	55.7 ± 1.2
zjet	1009.8 ± 3.4	37.8 ± 0.4	32.6 ± 0.5
diboson	228.5 ± 2.0	23.6 ± 0.4	23.4 ± 0.5
ttbar	453.3 ± 2.5	94.5 ± 1.0	108.2 ± 1.2
Expected	7023.0 ± 51.5	556.4 ± 8.9	353.1 ± 5.8
Data	7186	569	351

Table 6: Event yields after QCDNN>0.35 and TTNN>0.3 cuts that define the signal region. Only statistical uncertainties are reported

events. We use only events with at least one tight tag. According to the residual contributions of V+jets, QCD and $t\bar{t}$ found after the QCDNN and the TTNN cuts, the background is built with 90% untagged data and 10% $t\bar{t}$. As $t\bar{t}$ sample, we use $t\bar{t}$ events with at least one tight tag. We considered only processes contributing individually for more than 5% of the total background in events with at least one tag. We re-weighted the contributions of the single process in order to provide a complete background set (100%). The multivariate technique used here is again MLP. Our network has 2 hidden layers. The nodes of each layer are 7:10:7:1. The neuron activation function is the hyperbolic tangent. We use a LearningRate of 0.01 and a TestRate of 5. The other parameters are set to the default in TMVA. We train for 500 epochs. The 7 used variables are:

- QCDNN.singletop=the QCDNN output
- JET.pt2=the transverse momentum of the second jet
- MASS.mvj2=transverse mass of the missing transverse energy and the second jet
- MVJ123=transverse mass of the missing transverse energy and all jets
- MET.ht=sum of jets E_T
- MASS.mvj12=transverse mass of the missing transverse energy and of the two leading jets
- MET.sumjetpt=sum of the jet transverse momenta

Fig. 7, 8 show the MLP output, which still does a good job at discriminating signal from background.

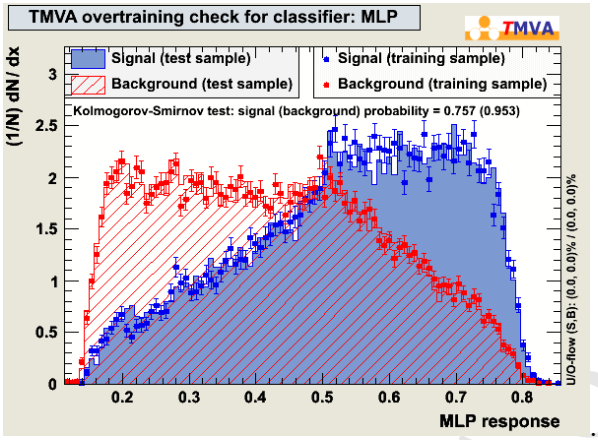

Figure 7: SIGNN output for the testing and training samples

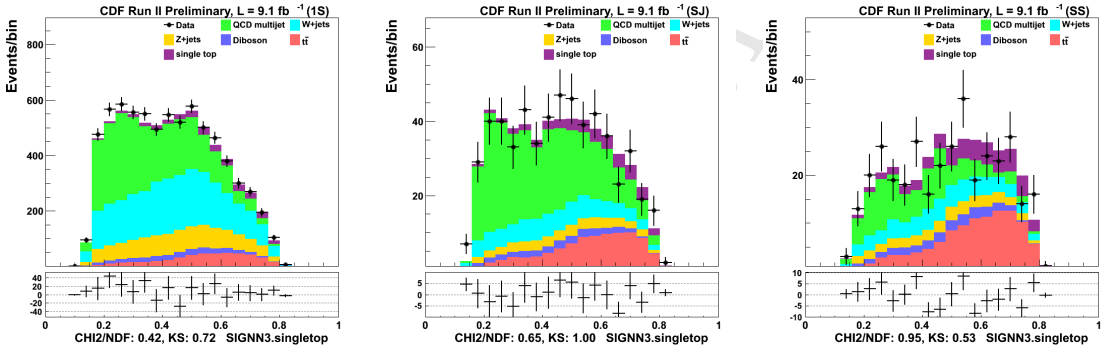

Figure 8: SIGNN stack plots in 1S, SJ, SS regions with subtraction plots on bottom.

5 Cross Section Measurement

Single top signal is extracted performing a bayesian fit of SIGNN distribution. `MCLIMIT` package [22] is used for this purpose. The fit is performed simultaneously in the 3 different tagging categories 1S, SJ, SS.

5.1 Systematics

In this section we describe the systematic uncertainties that were considered. In Table 7 are summarized the systematics considered for each template.

- **Cross Section Uncertainty**. Since rate is predicted in a specific way for each processes, a specific rate systematics is applied for every template
  - single top: our signal normalization is allowed to float unconstrained in the fit, adding no rate systematics for it.

  - diboson: we constrain the diboson normalization to its predicted cross section with an uncertainty of 6%.
  - $t\bar{t}$: since we constrain the $t\bar{t}$ normalization using the measured cross-sections (7.71±0.51 pb [16]), we apply a 6.6% uncertainty on top-antitop production rate.
  - V+jets (V = W,Z): we allow the V +jets background rates to float unconstrained in each tagging category. We then apply no rate systematics for V+jets production.
  - QCD: the normalization derived from the fit in QCDNN (Section 3.4.1) is constrained within 20%. Being inspired by what was done in the implementation of Method2 [17], this conservative 20% uncertainty is taken on the QCD fraction as opposed to using the under-estimated uncertainty from the fitted results.

- **Luminosity Uncertainty**. The procedure for determining the uncertainty on the luminosity for Run 2 until August 2004 is described in [19]. This uncertainty amounts to 6% and applies to those simulations that are normalized to luminosity. This uncertainty does not apply to the QCD and V+jets, which are data-driven, and $t\bar{t}$, because we use the measured cross section.

- **PDF Uncertainty**. The PDF uncertainty has been determined using the method that is described in [20]. In earlier analyses [21], it has been determined that a 2% uncertainty on the acceptance due to the choice of the PDF is sufficient.

- **Jet Energy Scale Uncertainty**. The Jet Energy Scale uncertainty was determined by varying the jet energy correction factor by plus or minus one sigma. This variation then propagates to the $\not\!\!E_T$ reconstruction, the calculation of the azimuthal direction of $\not\!\!E_T$ and thus to the expected number of events after applying the selection cuts. The influence of this variation is different for each background component; therefore, it needs to be determined separately by running the entire analysis code twice on all the simulated backgrounds. Since in this analysis we use the H1 algorithm to correct jet energies, additional systematic uncertainties need to be assigned. This is done by varying pT of the tracks used in the H1 algorithm by 3% [13]. The JES uncertainty can also modify the shape of the distributions. In some cases, the JES can be very asymmetric. In the cross section calculation the $\pm 1\sigma$ shapes and rates are obtained for backgrounds and signal, thus taking the asymmetric nature of the uncertainty into account.

- **Renormalization and Factorization Scales in the W +jets MC (Q^2)**. The `ALPGEN` event generator used for W +jets events requires renormalization and factorization scales of the Q^2 parameter to be chosen appropriately to account for the finite order perturbative calculations of cross sections and for the factorization approximation of structure functions and cross sections. Since the Q^2 values are

not known, and indeed not physically measurable since they are an artifact of the theoretical approximation, an uncertainty is assigned to cover a variety of different possibilities. As a default, the renormalization and factorization scales are set to be the same at $Q^2 = M_W^2 + \Sigma p_T^2$, where M_W is the W boson mass and p_T^2 is the parton transverse momentum squared. The sum extends over all final state partons [23]. This parameter is doubled and halved to create two samples which are used to determine the shape uncertainty on the W +jets template[6].

- **B-tagging scale factor**. The efficiency of tagging a taggable jet in the simulation is different from that in real events. This difference has to be taken into account when calculating the predicted number of events in the simulation after requiring a tag. For tight SecVTX tagger the scale factor is 0.96 ± 0.05 as it is described on High-Pt Btag web page. For JetProbability tagger (< 5% operating point) the Data-MC scale factor reported is 0.77 ± 0.04. The scale factors that are actually used, labeled SS', SJ', 1S' according to John Freeman's convention, are defined as:

  - SS' = 0.92 × N_{SS}
  - SJ' = 0.74 × N_{SJ} + 0.05 × N_{SS}
  - 1S' = 0.96 × N_{1S} + 0.22 × N_{SJ} + 0.03 × N_{SS}

  Where N_{1S}, N_{SJ} and N_{SJ} are the uncorrected predicted rates before applying any scale factor. We then define two different systematics, one for the SecVTX tagger, the other one for the JetProbability tagger, based on the uncertainties reported on High-Pt Btag web page. These two uncertainties where considered in order to take into account the correlation between the different tagging categories:

  - SecVtx unc: 1S'=±5.2%, SS'=±10.4%, SJ'=∓3%
  - JetProb unc: 1S'=∓3%, SS'=±0%, SJ'=±3.3%

- **Trigger Efficiency**. The trigger efficiency study is described in [24]. Since we are now using data below the region of full efficiency, we assign a systematic uncertainty to both MC based backgrounds and signal acceptances, by varying the trigger efficiency by $\pm 1\sigma$.

- **Lepton Veto**. The uncertainty in the efficiency of these cuts was determined to be safely accounted for by assuming ±2% [12].

- **ISR/FSR**. The uncertainty associated with the initial and final state radiation was evaluated for the signal by generating samples with more/less ISR/FSR according to the Joint Physics recommendation. This uncertainty is applied only to single top.

[6] This method addresses the shape uncertainty only. Since the theoretical cross section of W +jets is only known to the lowest order in QCD and suffers from large uncertainties, its normalization is derived from data

- **Top mass dependence**. We consider top masses of 170 & 180 GeV as $\pm 2\sigma$ variations. This uncertainty is applied to all top processes.

- **TRF**. There is an uncertainty in the tag rate function parameters. This is only considered for the QCD multijet background. The variations in TagRateMatrix, which is used to estimate the multijet background, can also modify the distributions. It is taken into account by varying the tag-rate probability in each bin of the matrix by $\pm 1\sigma$, and the alternative shapes are used in the limit calculation.

Systematic	Region	Signal	diboson	$t\bar{t}$	V+jets	QCD
Luminosity	1S+SJ+SS	$\pm^{6\%}_{6\%}$	$\pm^{6\%}_{6\%}$	no	no	no
PDF	1S+SJ+SS	$\pm^{2\%}_{2\%}$	$\pm^{2\%}_{2\%}$	no	no	no
Lepton veto	1S+SJ+SS	$\pm^{2\%}_{2\%}$	$\pm^{2\%}_{2\%}$	no	no	no
B-tagging SecVTX	1S	$\pm^{5.2\%}_{5.2\%}$	$\pm^{5.2\%}_{5.2\%}$	$\pm^{5.2\%}_{5.2\%}$	no	no
	SJ	$\mp^{3\%}_{3\%}$	$\mp^{3\%}_{3\%}$	$\mp^{3\%}_{3\%}$	no	no
	SS	$\pm^{10.4\%}_{10.4\%}$	$\pm^{10.4\%}_{10.4\%}$	$\pm^{10.4\%}_{10.4\%}$	no	no
B-tagging JetProb	1S	$\mp^{3\%}_{3\%}$	$\mp^{3\%}_{3\%}$	$\mp^{3\%}_{3\%}$	no	no
	SJ	$\pm^{3.3\%}_{3.3\%}$	$\pm^{3.3\%}_{3.3\%}$	$\pm^{3.3\%}_{3.3\%}$	no	no
	SS	$\mp^{0\%}_{0\%}$	$\mp^{0\%}_{0\%}$	$\mp^{0\%}_{0\%}$	no	no
Cross Section	1S+SJ+SS	no	$\pm^{6\%}_{6\%}$	$\pm^{6.6\%}_{6.6\%}$	no	$\pm^{20\%}_{20\%}$
JES shape/rate	1S	yes/$\pm^{4\%}_{4\%}$	yes/$\pm^{6\%}_{6\%}$	yes/$\mp^{2\%}_{2\%}$	yes/no	no/no
	SJ	yes/$\pm^{4\%}_{4\%}$	yes/$\pm^{5\%}_{5\%}$	yes/$\pm^{1\%}_{1\%}$	yes/no	no/no
	SS	yes/$\pm^{3\%}_{3\%}$	yes/$\pm^{6\%}_{6\%}$	yes/$\pm^{1\%}_{1\%}$	yes/no	no/no
Q^2 scale	1S+SJ+SS	no	no	no	yes (only W+jets)	no
TRF	1S+SJ+SS	no	no	no	no	yes
ISR/FSR	1S+SJ+SS	$\pm^{2\%}_{2\%}$	no	no	no	no
Top mass dependence	1S+SJ+SS	yes	no	yes	no	no
Trigger efficiency	1S+SJ+SS	$\pm^{2\%}_{2\%}$	$\pm^{2\%}_{2\%}$	$\pm^{2\%}_{2\%}$	no	no

Table 7: Systematic uncertainties for 1S, SJ and SS regions for the templates used in the fits.

5.2 Results

We estimated the expected cross-section performing 20.000 pseudo-experiments with all systematics turned on (we also performed 1.000.000 samplings of the systematics space during the MC integration of the systematics in `MCLIMIT`). Fig. 9 shows the spread of the outcomes of those pseudo-experiments.

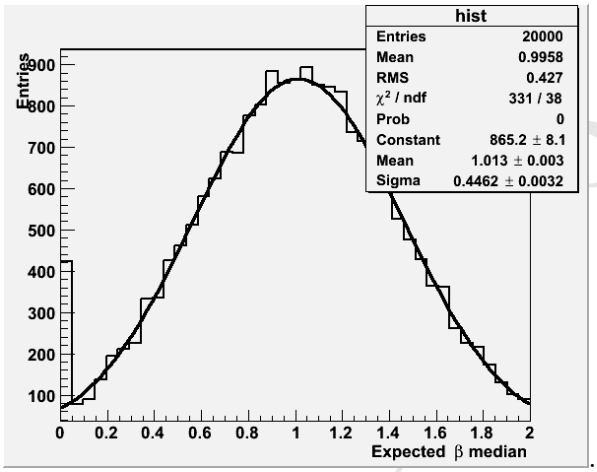

Figure 9: distribution of pseudo-experiments

After accounting for statistical and systematic errors, we expect a cross-section of:

$$\sigma_{exp}^{s+t} = 3.20^{+1.39}_{-1.43} \text{ pb} \quad (1)$$

Once this analysis is applied to 9.1 fb^{-1} of CDF Run II data, the observed cross-section is:

$$\sigma_{obs}^{s+t} = 3.04^{+1.46}_{-1.39} \text{ pb} \quad (2)$$

In Table 8 the pulls of the nuisance parameters are shown.

nuisance parameter	post-fit central value	post-fit uncertainty
BTAGSFSecVtx	-0.101523	± 0.789586
BTAGSFJetProb	-0.112227	± 0.980422
TTXSEC	-0.0664728	± 0.990537
JES	0.158143	± 1.00096
TRIGEFF	-0.0373967	± 1.00484
LUMI	-0.101581	± 0.988384
PDF	-0.0340026	± 0.998886
LEPTONIDVETO	-0.0312173	± 1.00656
DIBOSONXSEC	-0.0176684	± 0.991544
QCDXSEC	0.0704846	± 0.366264
TRFSHAPE	-0.148286	± 0.848294
VJETSXSEC	0.014009	± 0.0714255
Q2WJET	-0.0863352	± 0.473566
mcmcssf	1.00823	± 0.443342

Table 8: Pulls of the nuisance parameters.

6 Summary

We have presented a search for combined s- and t-channel electroweak single top production in the $\not\!\!E_T$+jets channel (events where the lepton from the W decay is either not identified or reconstructed as a jet). We have analyzed 9.1 fb^{-1} of CDF Run II data and measured the single top production cross-section:

$$\sigma_{obs}^{s+t} = 3.04^{+1.46}_{-1.39} \text{ pb} \quad (\sigma_{exp}^{s+t} = 3.20^{+1.39}_{-1.43} \text{ pb}) \tag{3}$$

A Control Regions

After the event preselection the data sample is mainly composed of multijet production (QCD+light flavour mistagged jets) processes. The high $\not\!\!E_T$ in these events comes both from a severe mis-measurement of one of the jets, which causes the missing energy to point along one of the jets, and from real sources of $\not\!\!E_T$ such as neutrinos or muons from semi-leptonic b-decays. We use a subset of the $\not\!\!E_T$+JETS sample to derive a model for these types of events [14] which will be used in the final signal region. We build three control regions, which we will use to test separately our data-driven and simulation-based background modeling.

A.1 Definitions

In order to test our ability to predict these backgrounds we check the performance of the method in two control regions. The first, `QCD` region, is a high statistics region where we check the data-based model and evaluate the systematic uncertainties on the shapes of various kinematic variables. Since in the Signal Region we expect backgrounds originating from events with real high $\not\!\!E_T$, such as W=Z+jets, $t\bar{t}$, single top production and diboson production, we test our ability to predict these backgrounds in another control region, the `EWK` region. In order to remain unbiased to our final region, we test EWK/Top backgrounds in the kinematic region similar to signal region, with the exception of requiring at least one lepton in the event (all events with leptons are vetoed in the signal region definition). This region is sensitive to ElectroWeak/Top processes, and is used to check the overall shapes of the Monte Carlo predictions. It also serves as an additional (but low statistics) check of the QCD model. The double-tagged events in this control region are dominated by the top processes, yielding an additional cross-check on top. In summary:

- `QCD` region:
  - All leptons are vetoed
  - $\Delta\phi(\not\!\!E_T, j_2) < 0.4$
  - $\not\!\!E_T > 70$ GeV (the 50 GeV $< \not\!\!E_T <$ 70 GeV region is used to build the Tag Rate Matrix for the multijet data-driven method)
- `EWK` region:
  - At least one loose lepton
  - $\Delta\phi(\not\!\!E_T, j_2) > 0.4$

A.2 Validation Plots in `QCD` region

We present a full set of validation plots in `QCD` region. The overall agreement between data and predictions is satisfying.

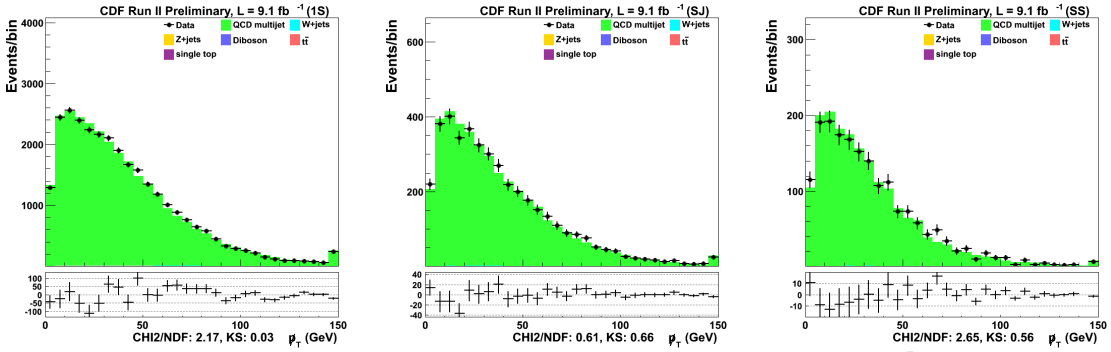

Figure 10: MPT stack plots in 1S, SJ, SS regions

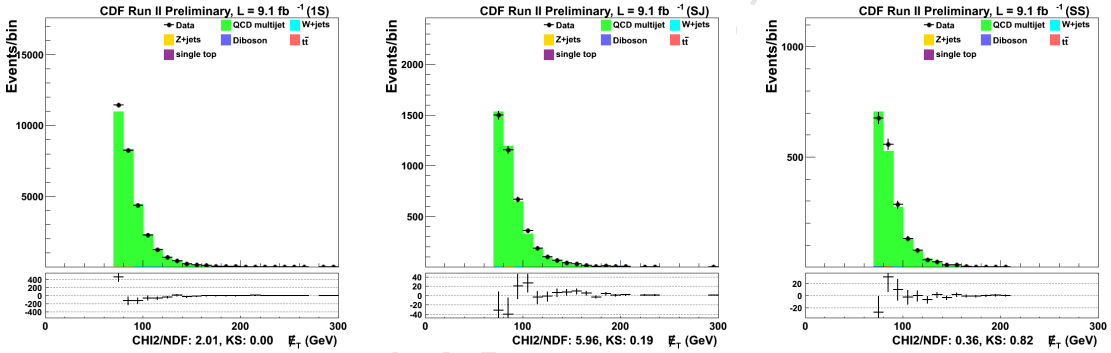

Figure 11: MET stack plots in 1S, SJ, SS regions

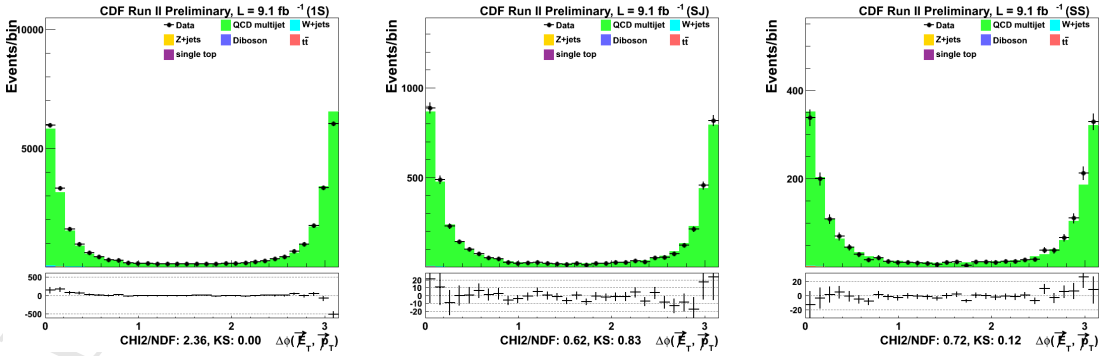

Figure 12: DPhiMET.MPT stack plots in 1S, SJ, SS regions

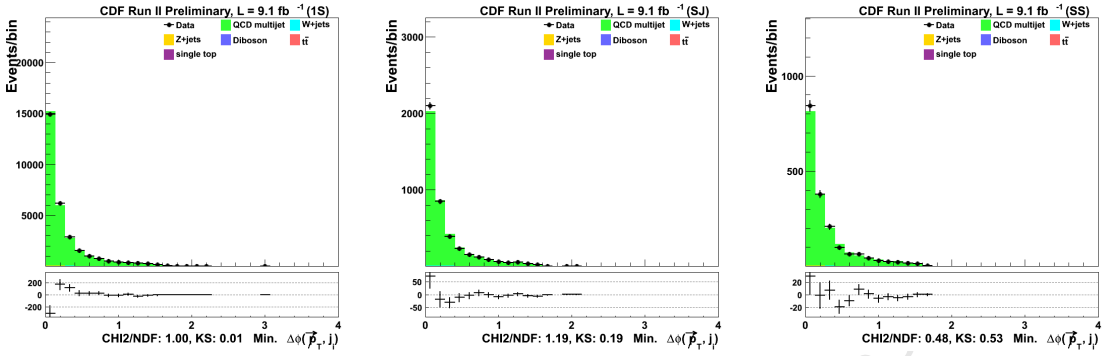

Figure 13: MinDPhiMPT.Ji stack plots in 1S, SJ, SS regions

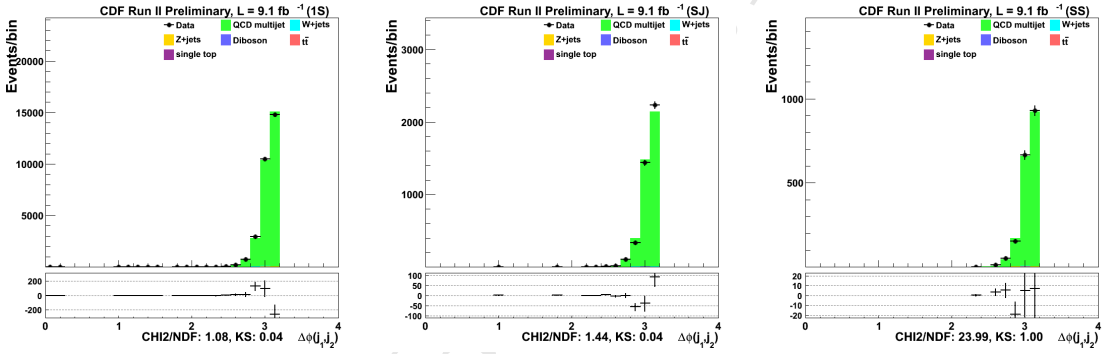

Figure 14: DPhiJ12 stack plots in 1S, SJ, SS regions

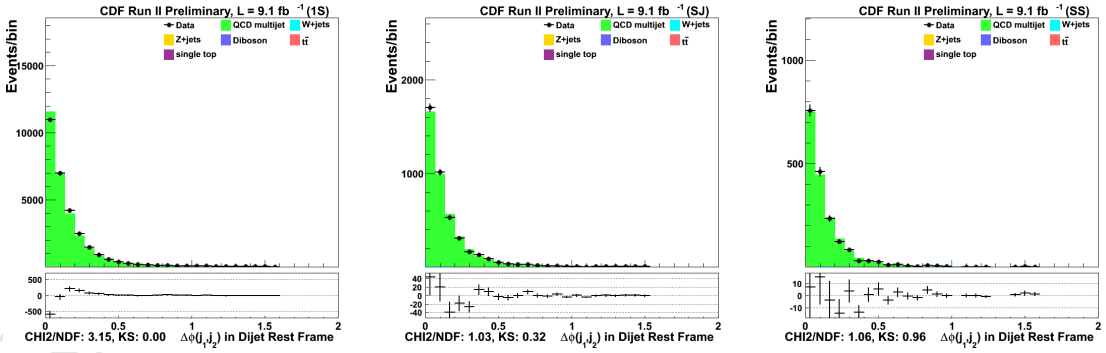

Figure 15: J12HRF stack plots in 1S, SJ, SS regions

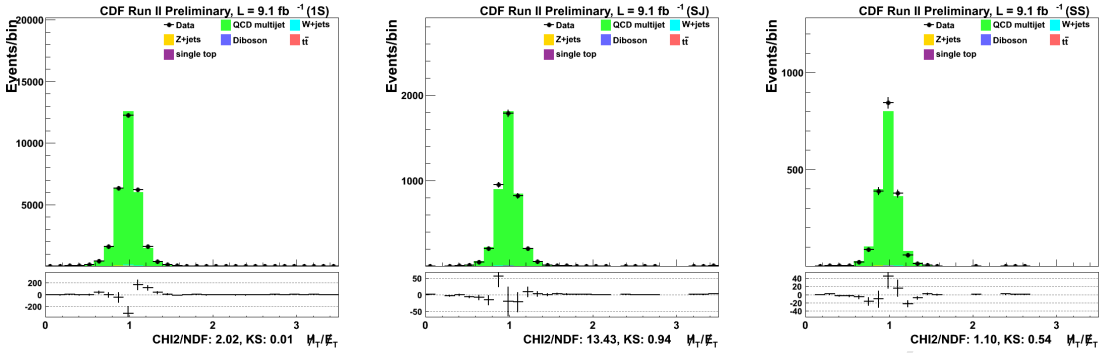

Figure 16: MHToMET stack plots in 1S, SJ, SS regions

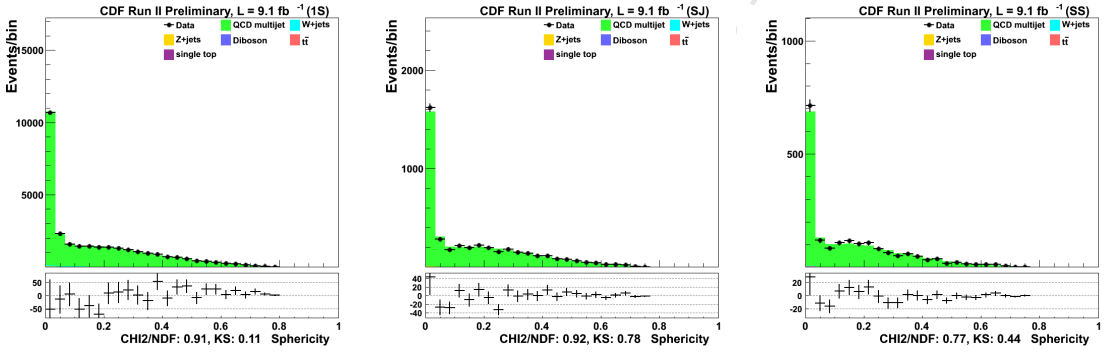

Figure 17: Sphericity stack plots in 1S, SJ, SS regions

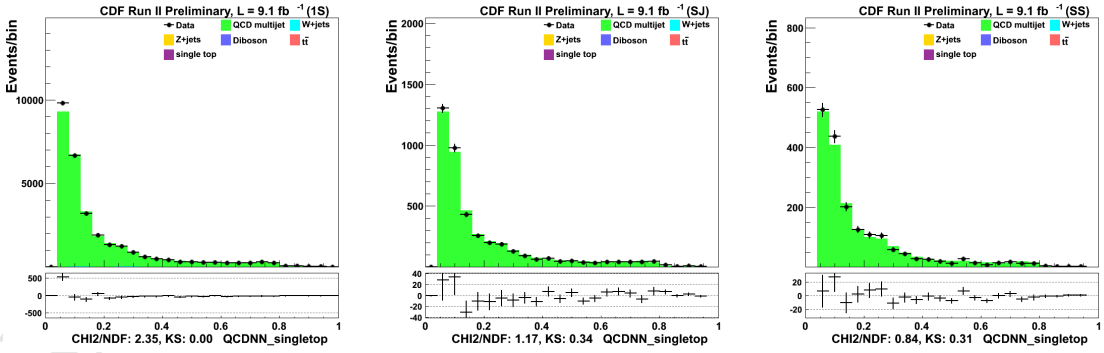

Figure 18: QCDNN.singletop stack plots in 1S, SJ, SS regions

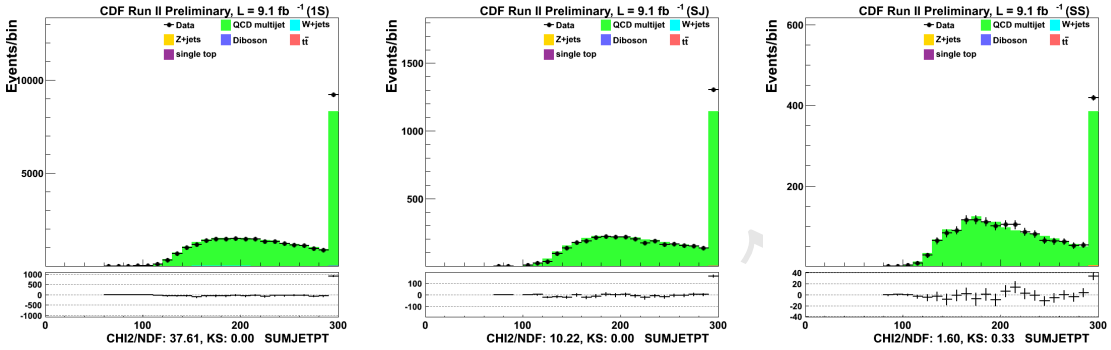

Figure 19: SUMJETPT stack plots in 1S, SJ, SS regions

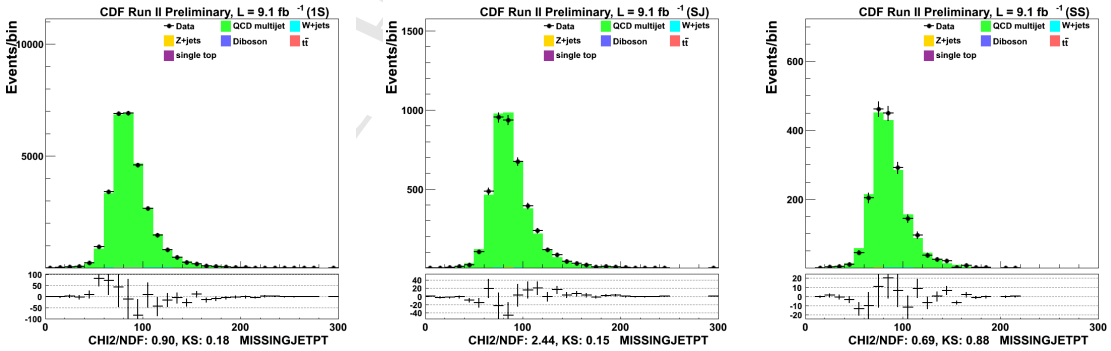

Figure 20: MISSINGJETPT stack plots in 1S, SJ, SS regions

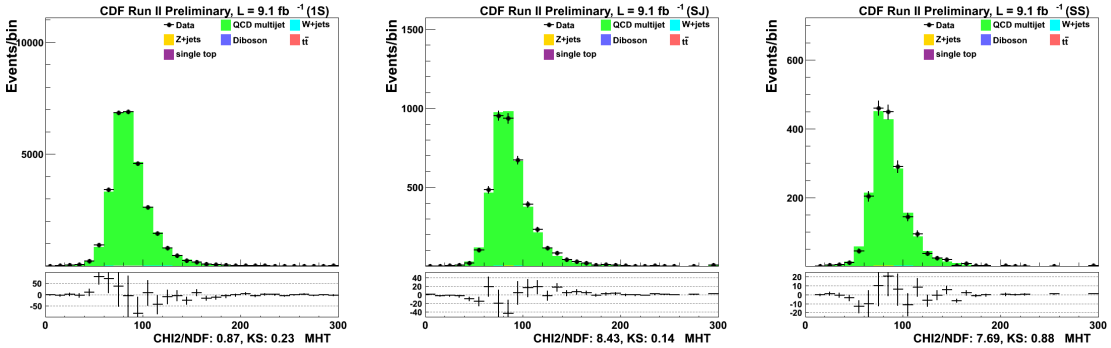

Figure 21: MHT stack plots in 1S, SJ, SS regions

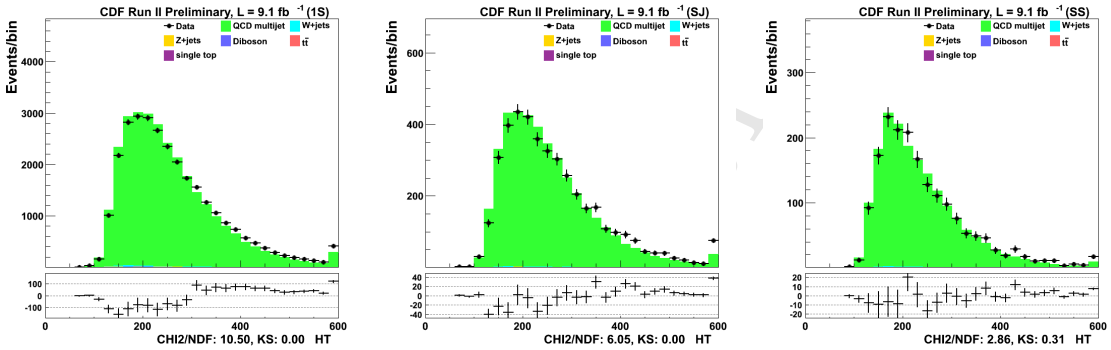

Figure 22: HT stack plots in 1S, SJ, SS regions

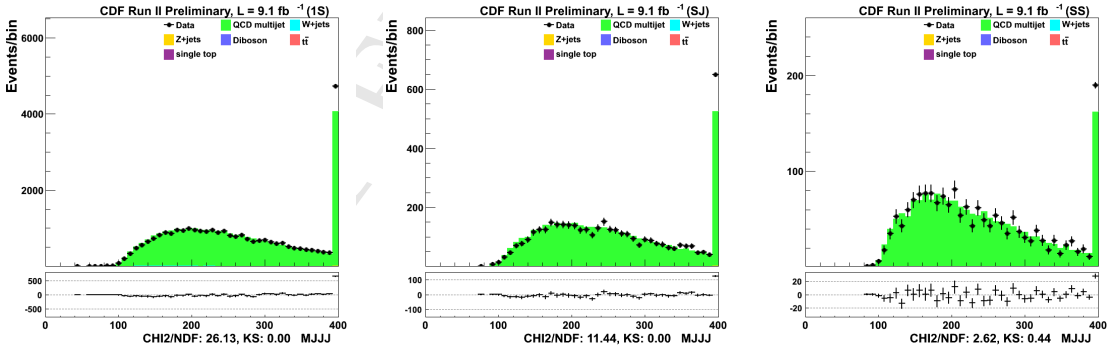

Figure 23: MJJJ stack plots in 1S, SJ, SS regions

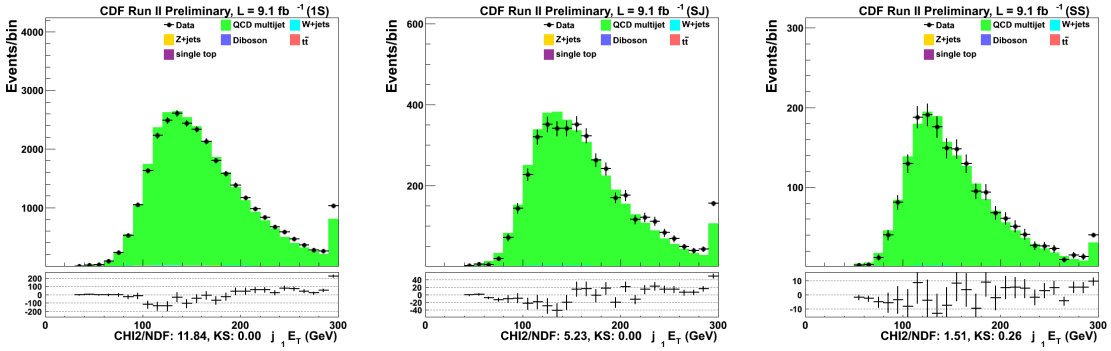

Figure 24: J1Et stack plots in 1S, SJ, SS regions

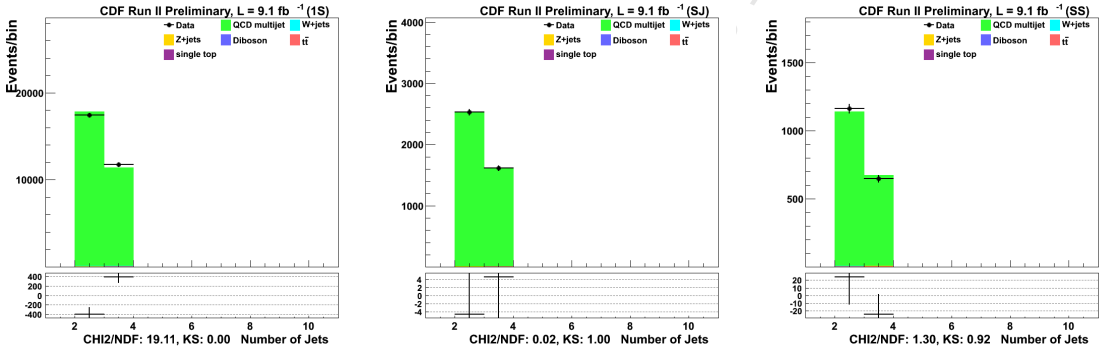

Figure 25: NJETS stack plots in 1S, SJ, SS regions

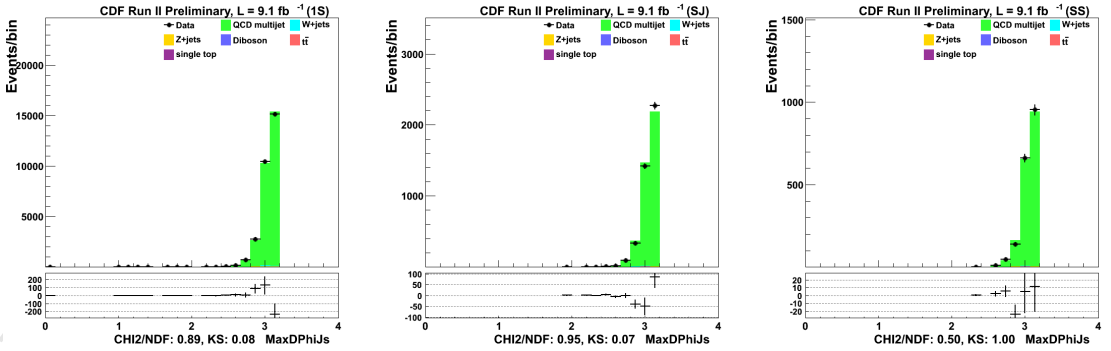

Figure 26: MaxDPhiJs stack plots in 1S, SJ, SS regions

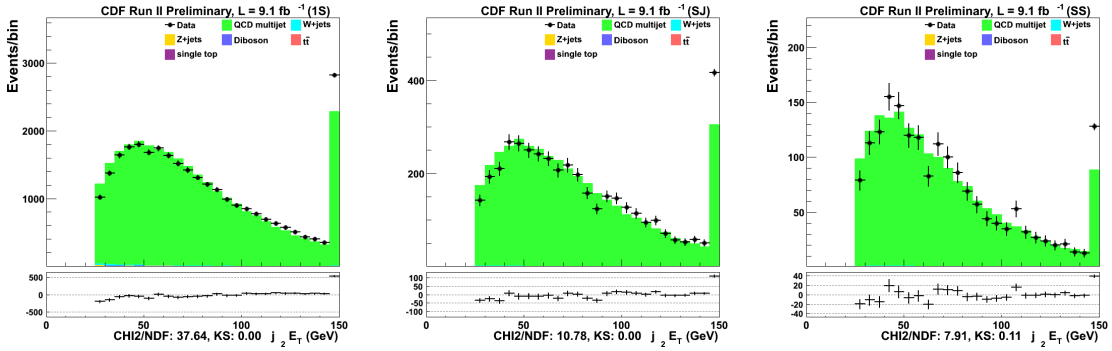

Figure 27: J2Et stack plots in 1S, SJ, SS regions

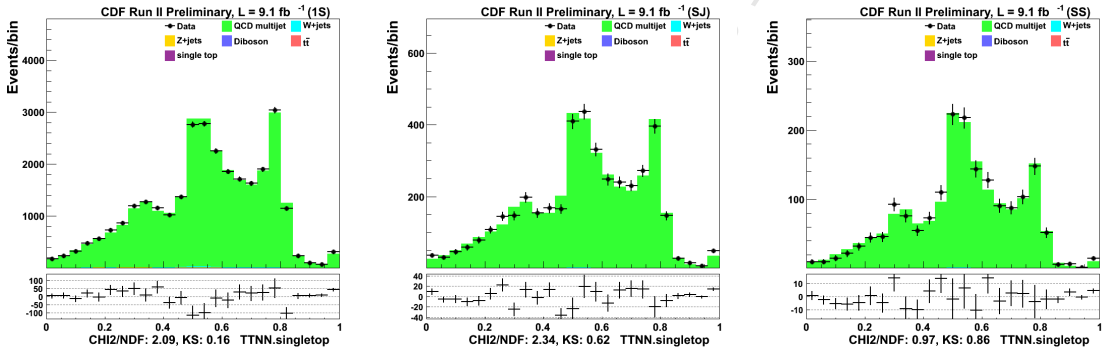

Figure 28: TTNN.singletop stack plots in 1S, SJ, SS regions

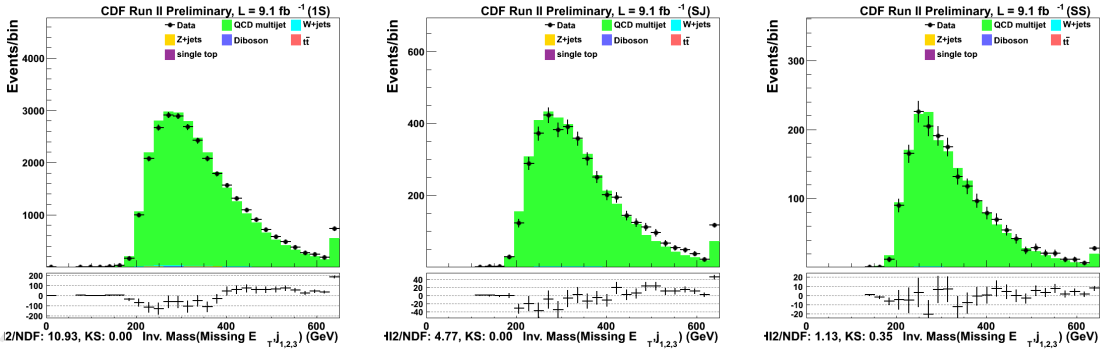

Figure 29: MVJ123 stack plots in 1S, SJ, SS regions

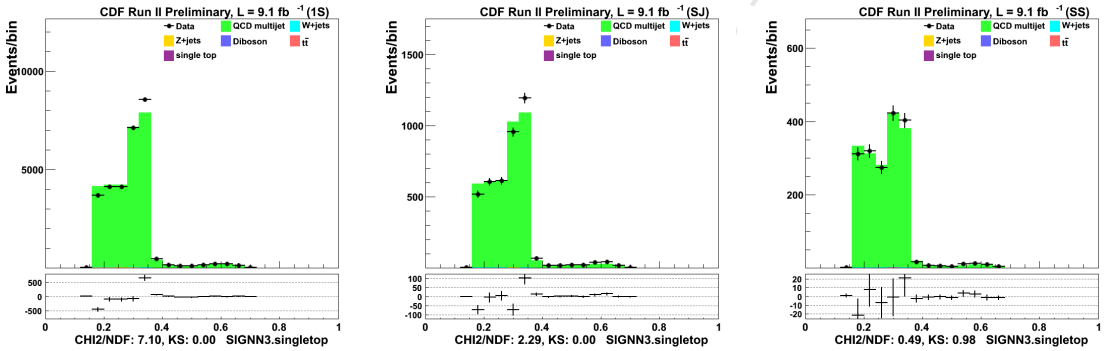

Figure 30: SIGNN3.singletop stack plots in 1S, SJ, SS regions

A.3 Validation Plots in EWK region

We present a full set of validation plots in EWK region. The overall agreement between data and predictions is satisfying.

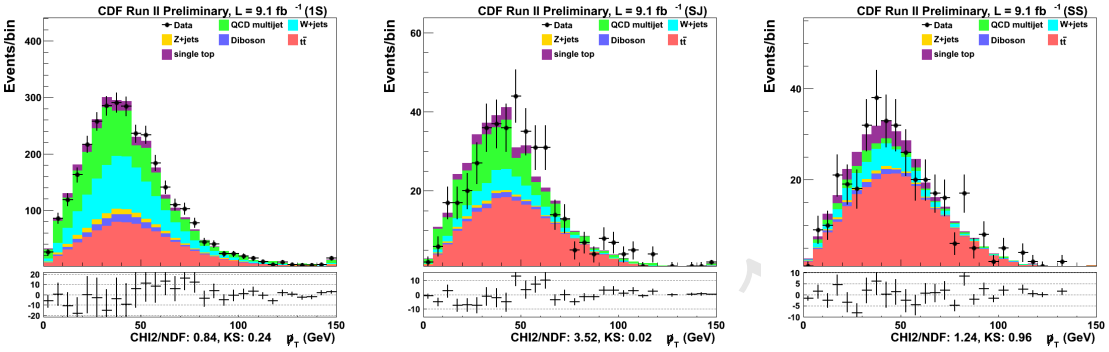

Figure 31: MPT stack plots in 1S, SJ, SS regions

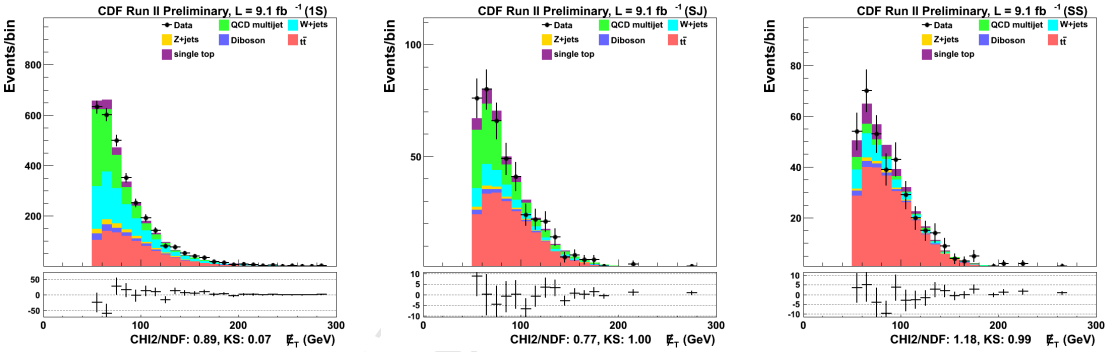

Figure 32: MET stack plots in 1S, SJ, SS regions

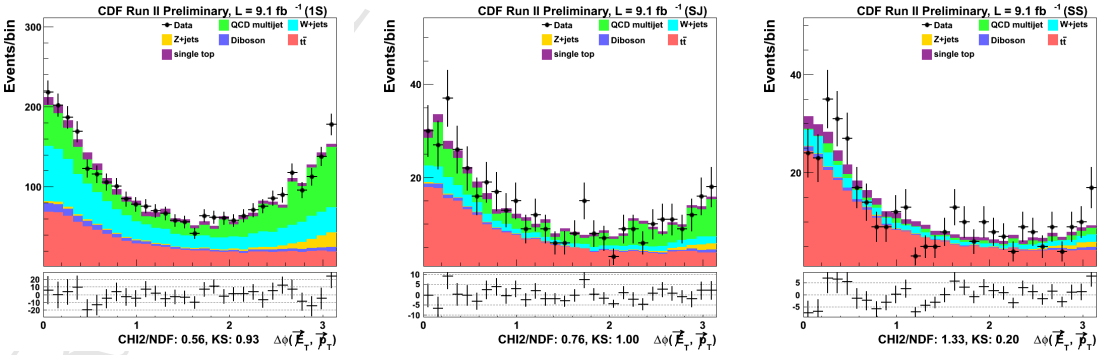

Figure 33: DPhiMET.MPT stack plots in 1S, SJ, SS regions

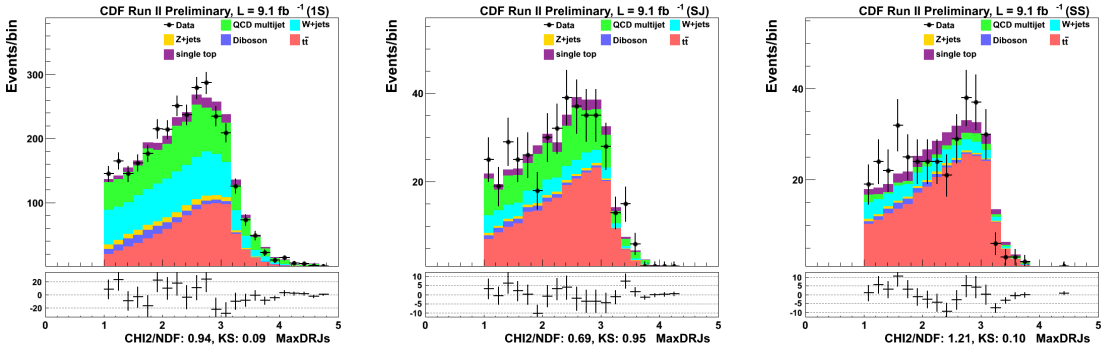

Figure 34: MaxDRJs stack plots in 1S, SJ, SS regions

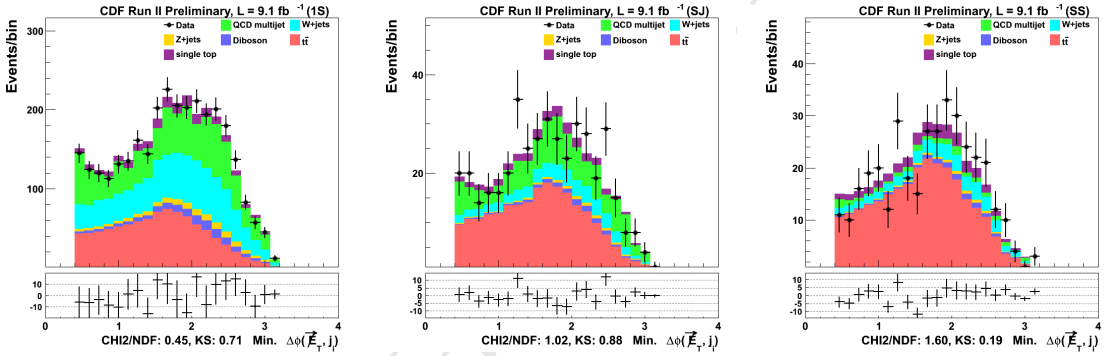

Figure 35: MinDPhiMET.Ji stack plots in 1S, SJ, SS regions

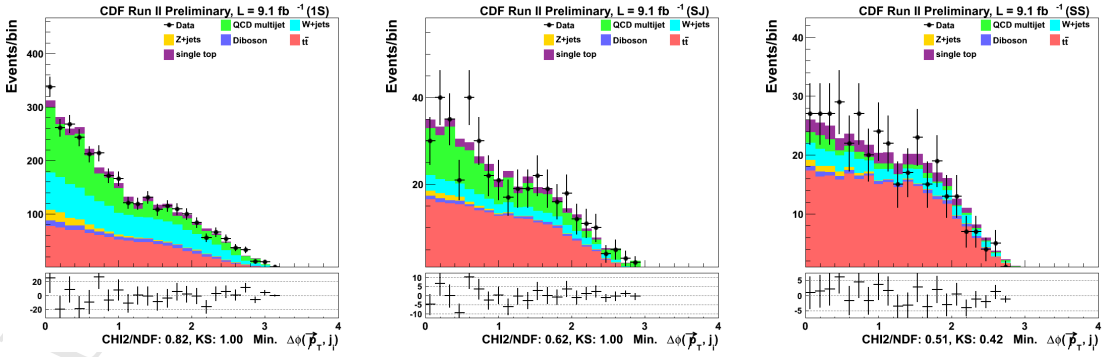

Figure 36: MinDPhiMPT.Ji stack plots in 1S, SJ, SS regions

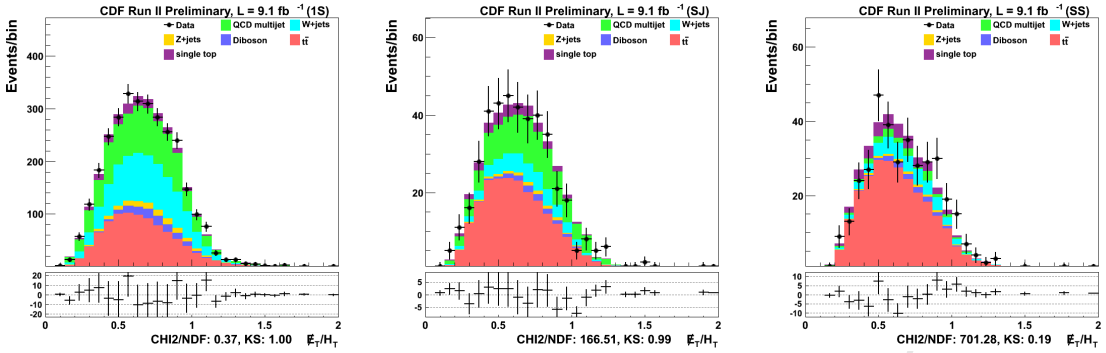

Figure 37: METoHT stack plots in 1S, SJ, SS regions

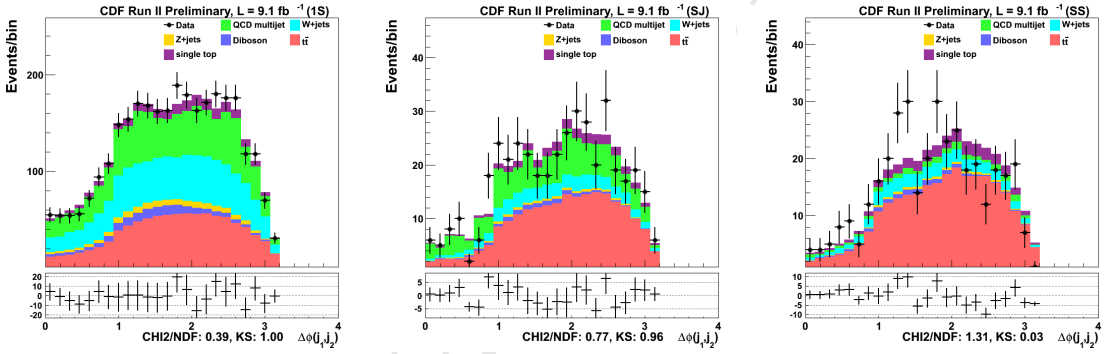

Figure 38: DPhiJ12 stack plots in 1S, SJ, SS regions

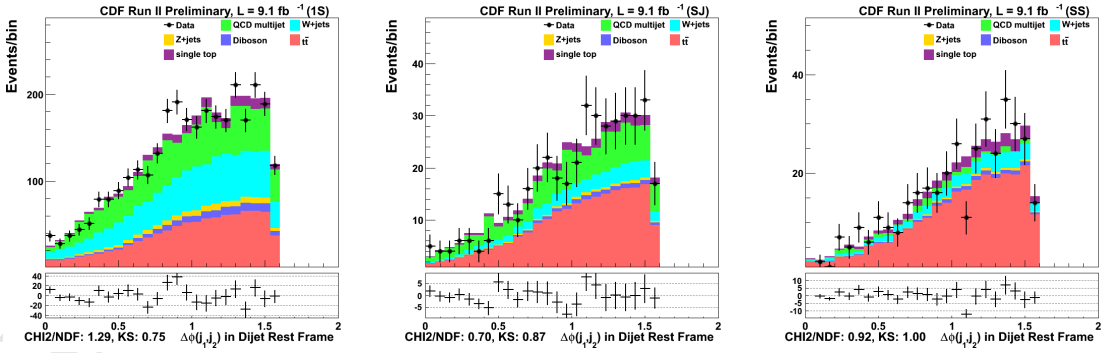

Figure 39: J12HRF stack plots in 1S, SJ, SS regions

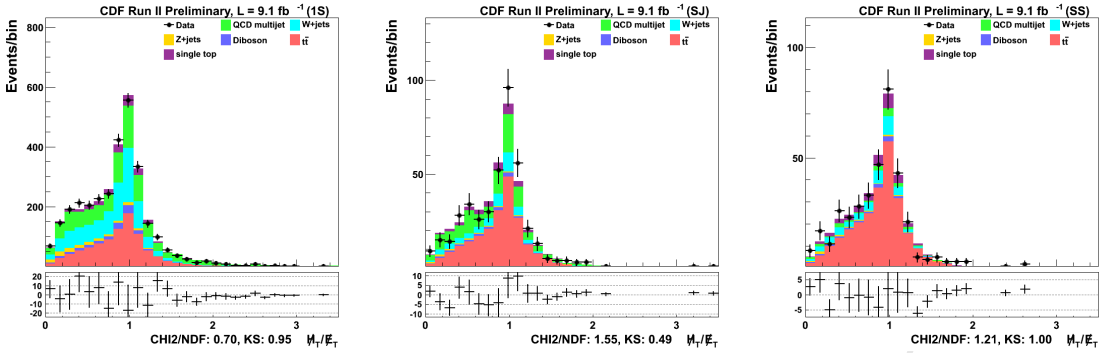

Figure 40: MHToMET stack plots in 1S, SJ, SS regions

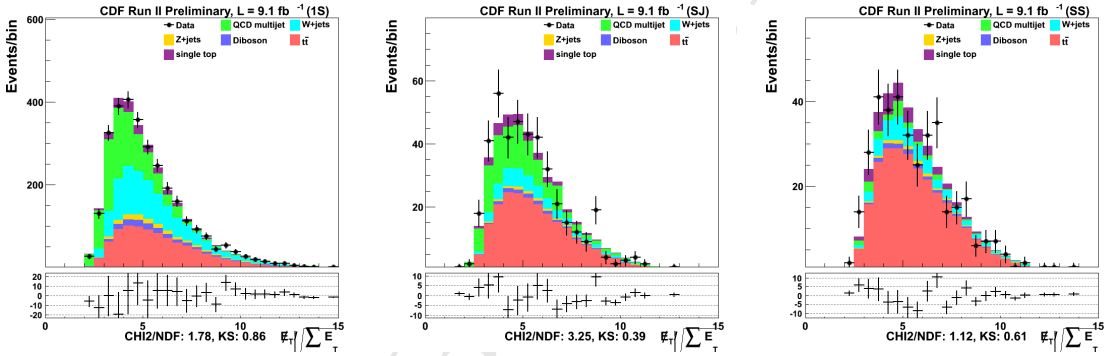

Figure 41: METsig stack plots in 1S, SJ, SS regions

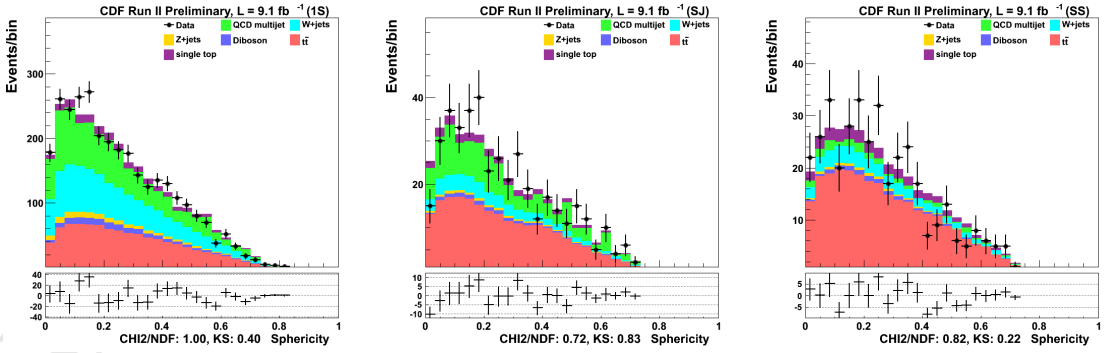

Figure 42: Sphericity stack plots in 1S, SJ, SS regions

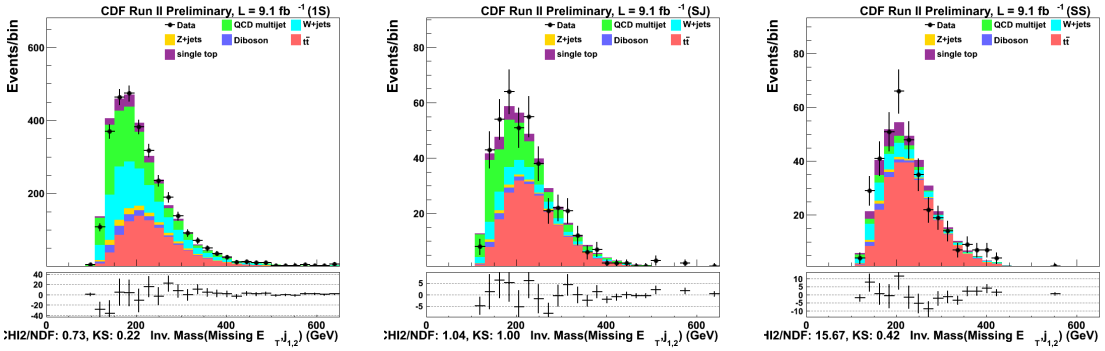

Figure 43: MVJ12 stack plots in 1S, SJ, SS regions

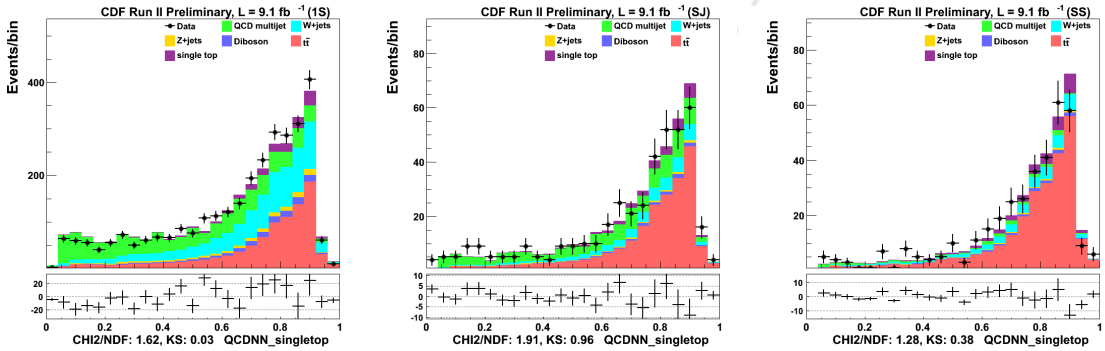

Figure 44: QCDNN.singletop stack plots in 1S, SJ, SS regions

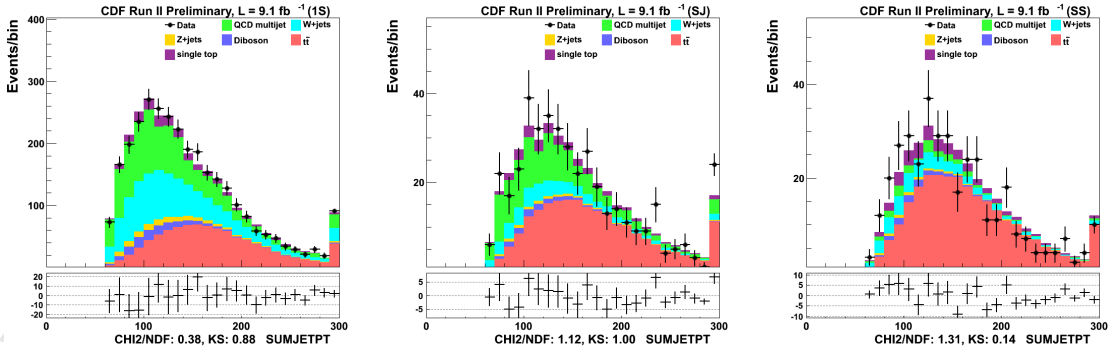

Figure 45: SUMJETPT stack plots in 1S, SJ, SS regions

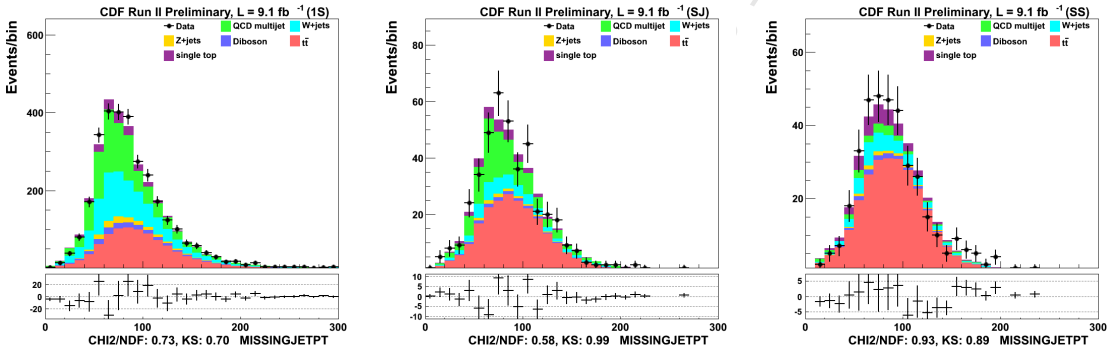

Figure 46: MISSINGJETPT stack plots in 1S, SJ, SS regions

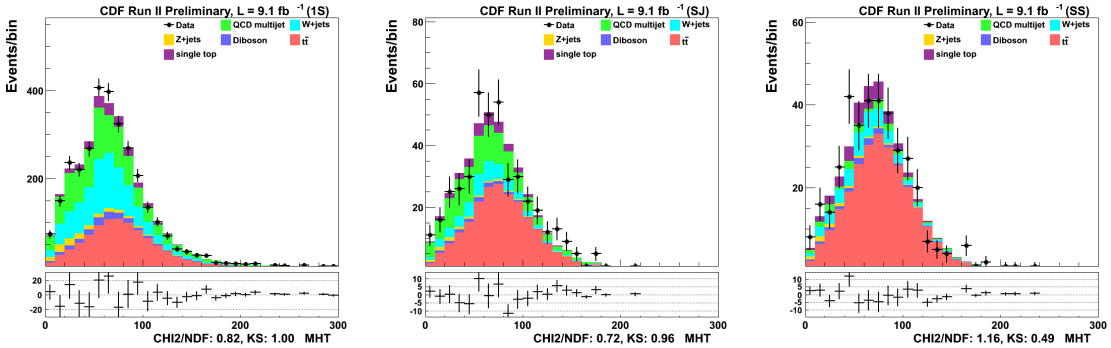

Figure 47: MHT stack plots in 1S, SJ, SS regions

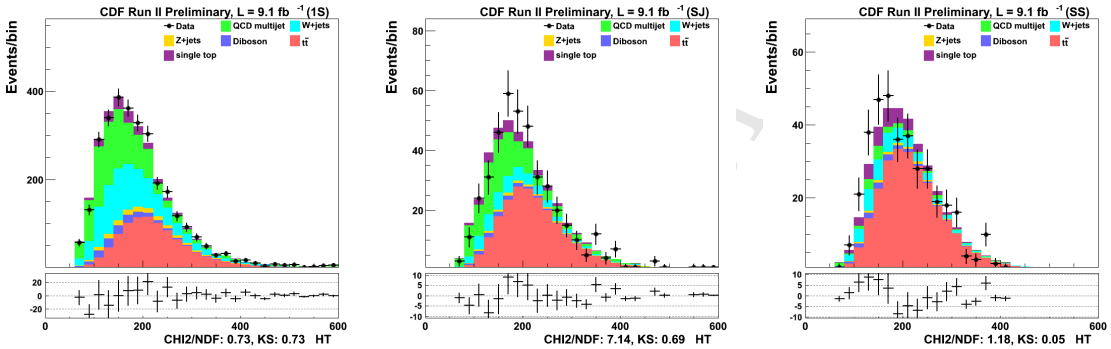

Figure 48: HT stack plots in 1S, SJ, SS regions

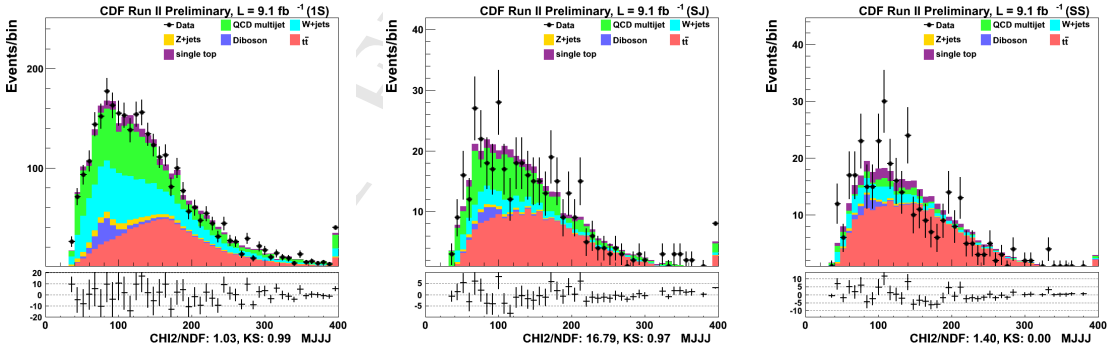

Figure 49: MJJJ stack plots in 1S, SJ, SS regions

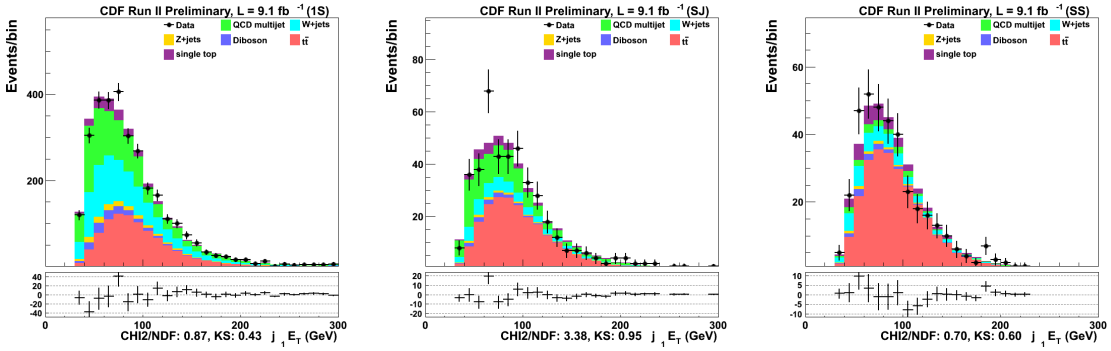

Figure 50: J1Et stack plots in 1S, SJ, SS regions

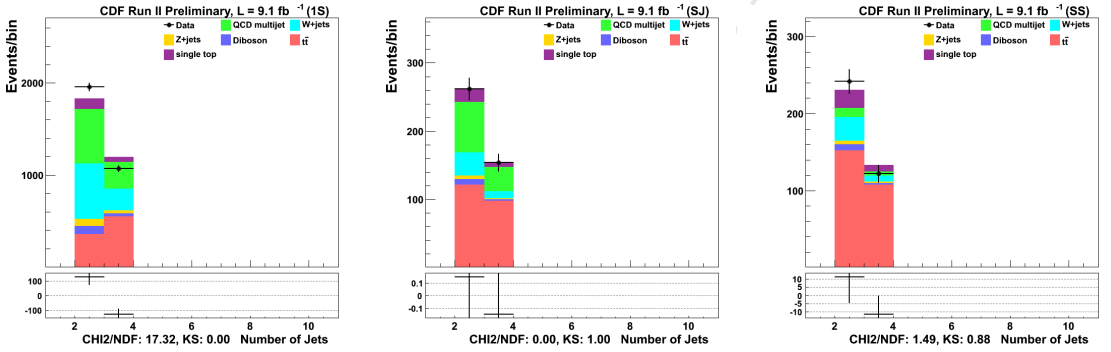

Figure 51: NJETS stack plots in 1S, SJ, SS regions

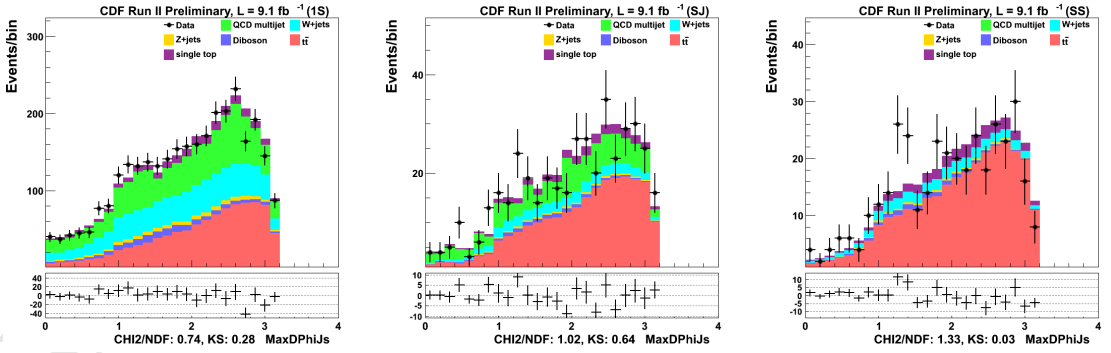

Figure 52: MaxDPhiJs stack plots in 1S, SJ, SS regions

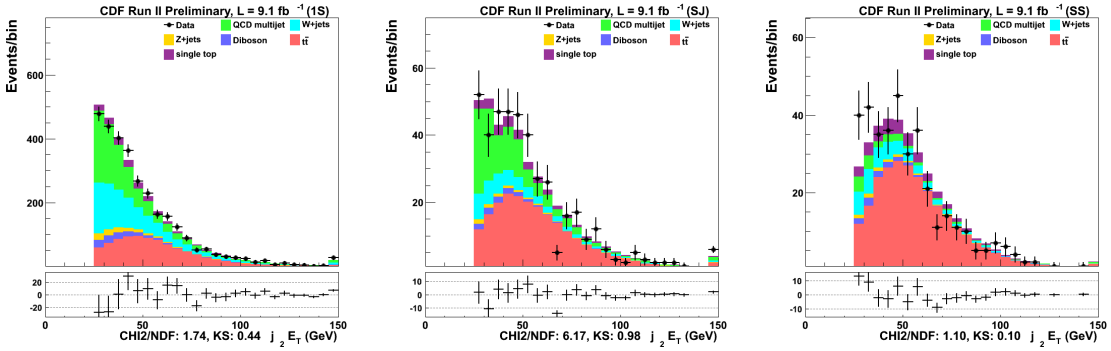

Figure 53: J2Et stack plots in 1S, SJ, SS regions

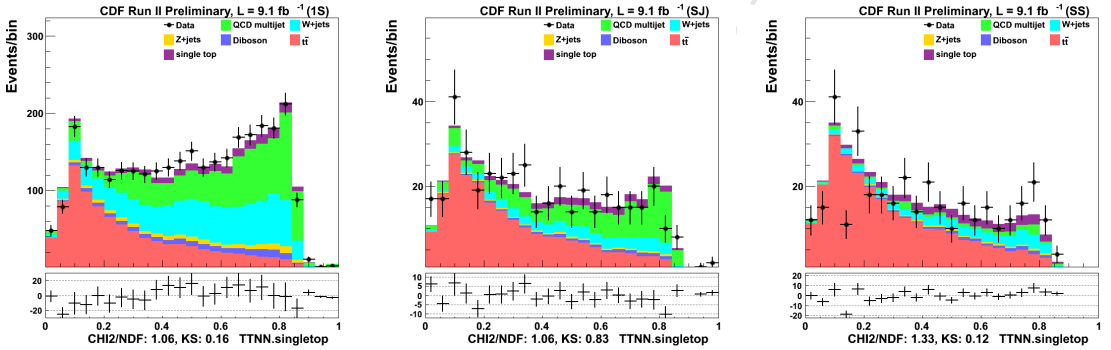

Figure 54: TTNN.singletop stack plots in 1S, SJ, SS regions

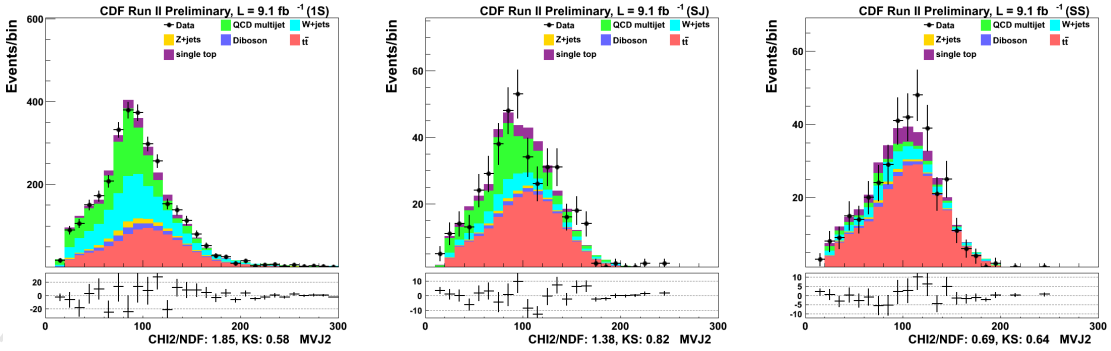

Figure 55: MVJ2 stack plots in 1S, SJ, SS regions

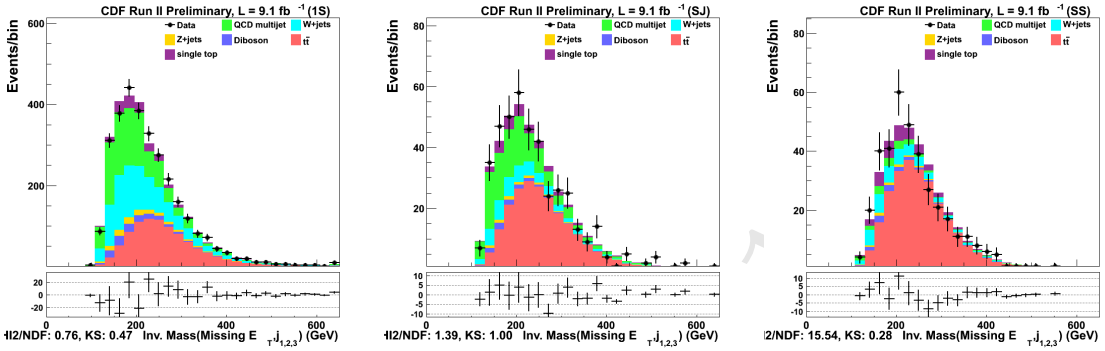

Figure 56: MVJ123 stack plots in 1S, SJ, SS regions

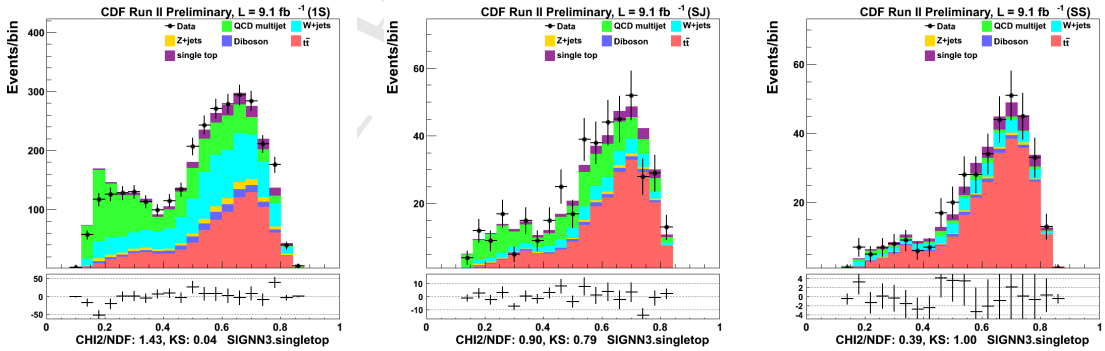

Figure 57: SIGNN3.singletop stack plots in 1S, SJ, SS regions

B QCDNN input variables

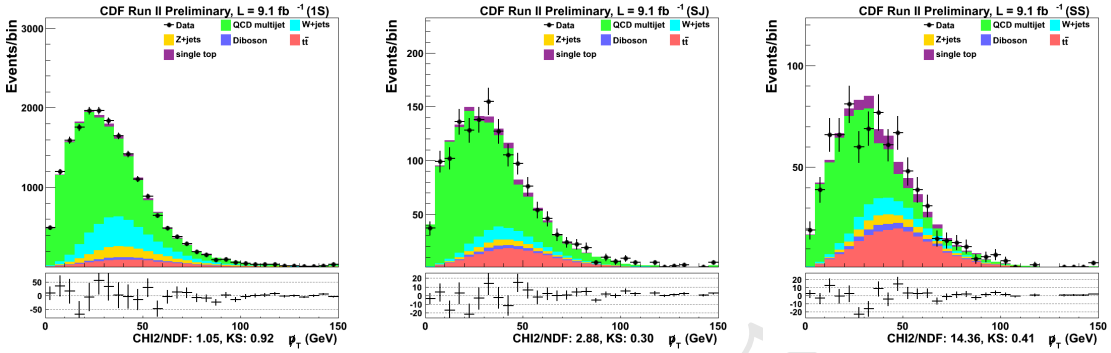

Figure 58: MPT stack plots in 1S, SJ, SS regions

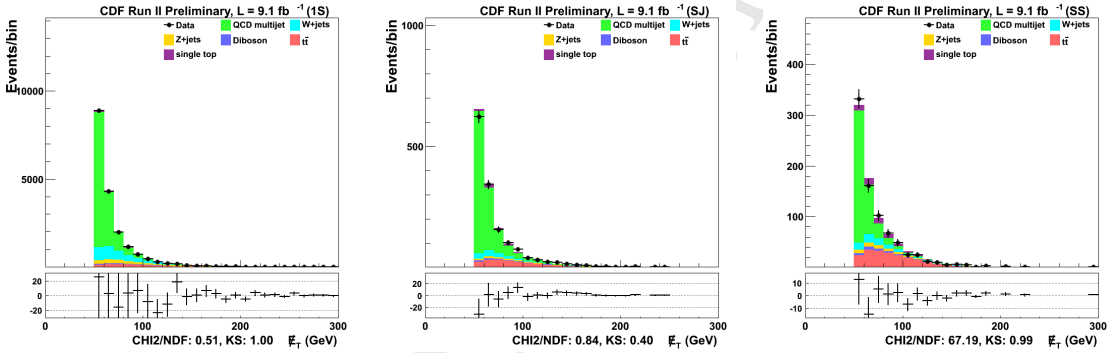

Figure 59: MET stack plots in 1S, SJ, SS regions

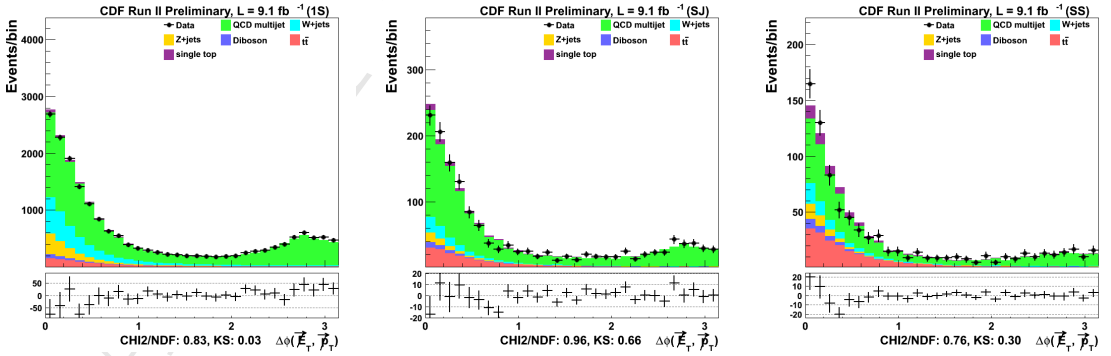

Figure 60: DPhiMET.MPT stack plots in 1S, SJ, SS regions

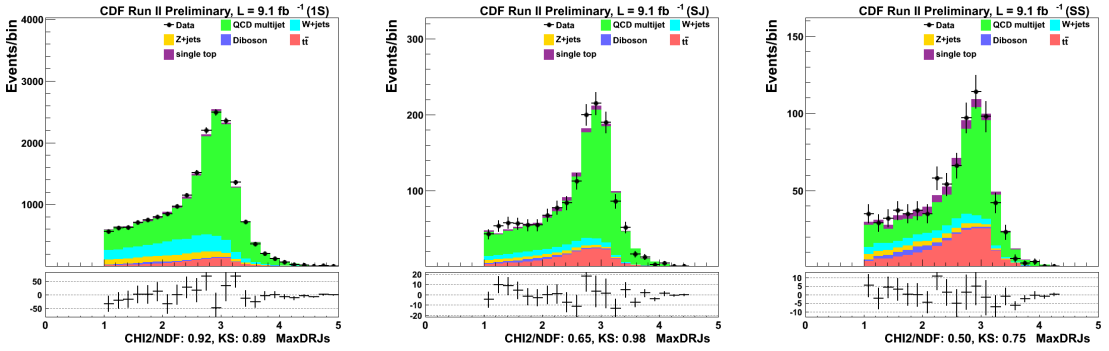

Figure 61: MaxDRJs stack plots in 1S, SJ, SS regions

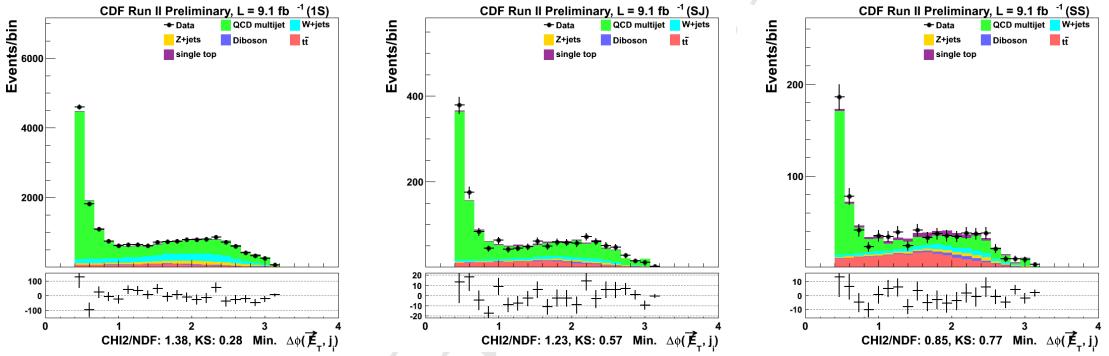

Figure 62: MinDPhiMET.Ji stack plots in 1S, SJ, SS regions

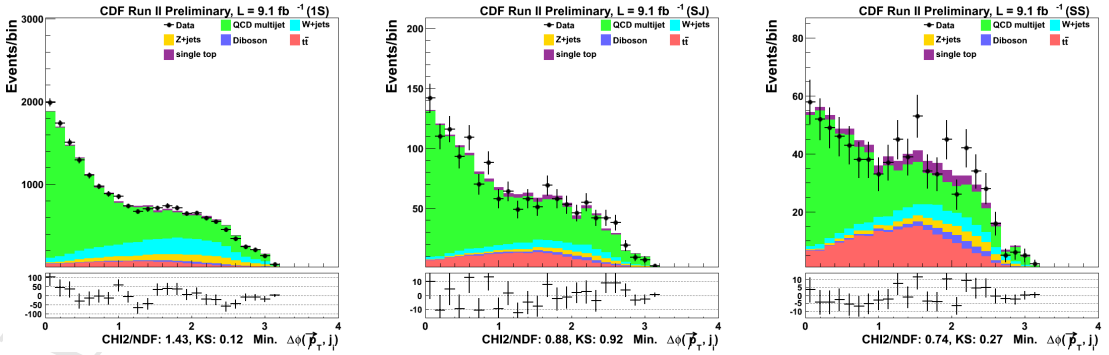

Figure 63: MinDPhiMPT.Ji stack plots in 1S, SJ, SS regions

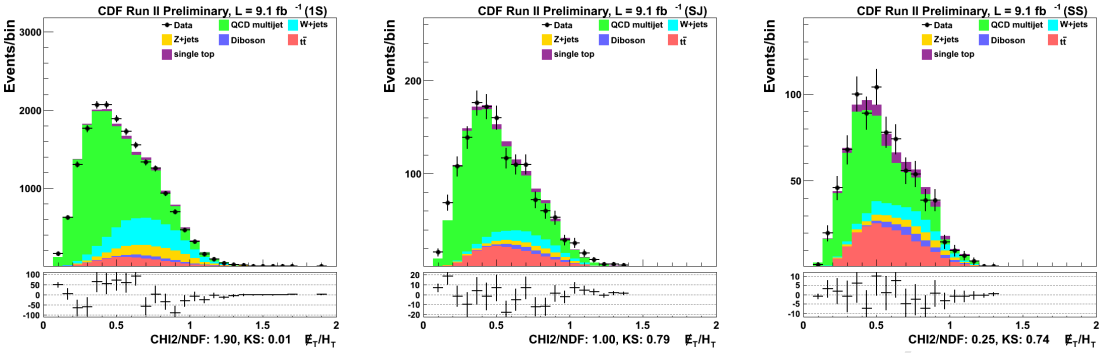

Figure 64: METoHT stack plots in 1S, SJ, SS regions

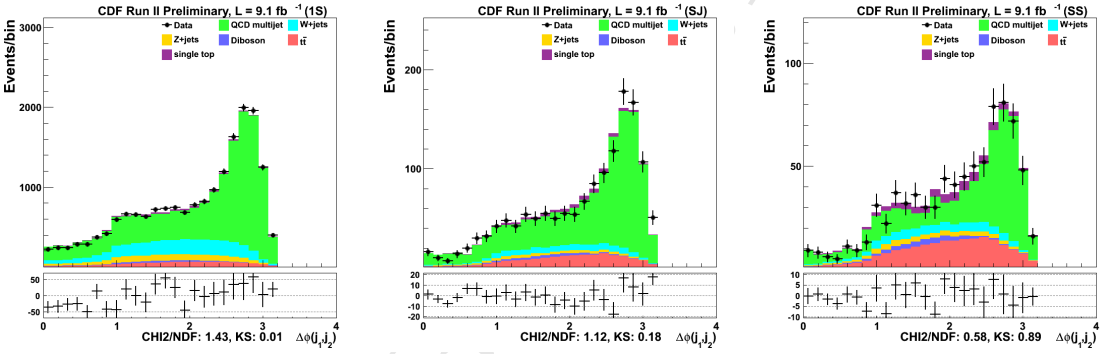

Figure 65: DPhiJ12 stack plots in 1S, SJ, SS regions

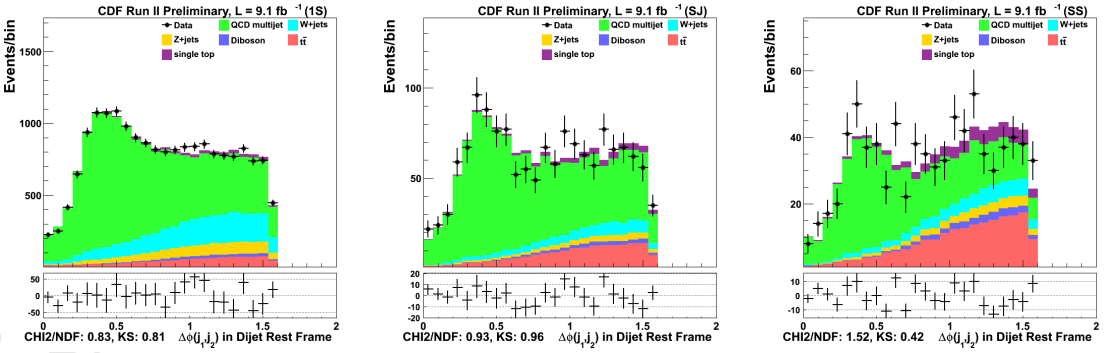

Figure 66: J12HRF stack plots in 1S, SJ, SS regions

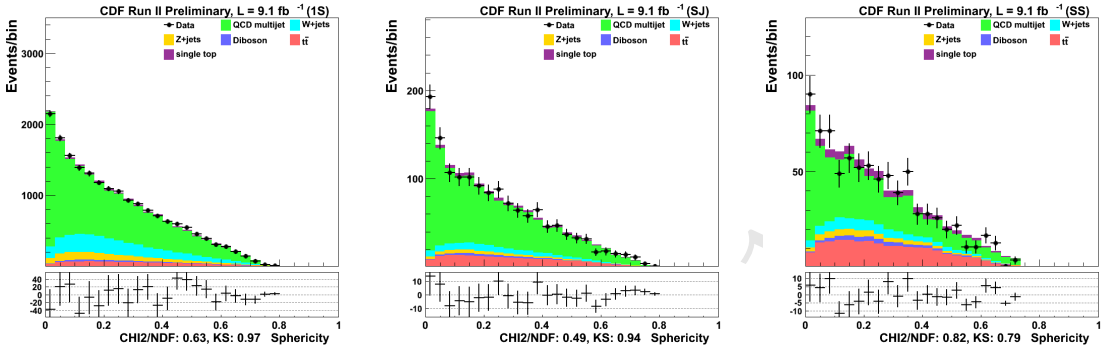

Figure 67: Sphericity stack plots in 1S, SJ, SS regions

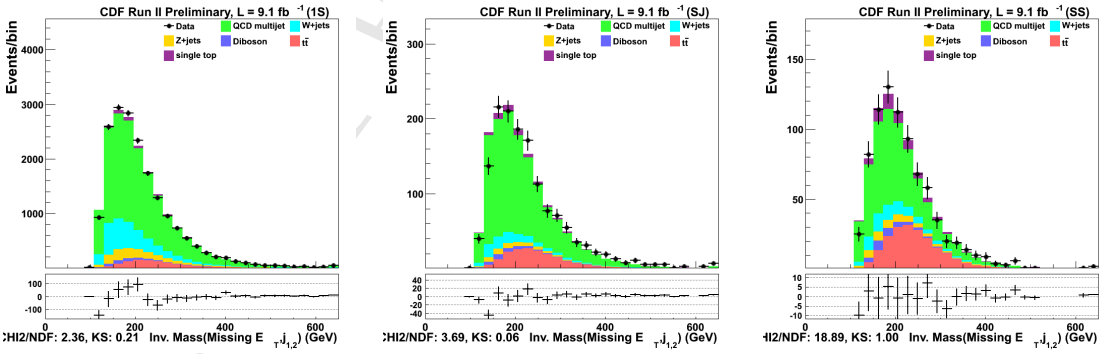

Figure 68: MVJ12 stack plots in 1S, SJ, SS regions

C TTNN input variables

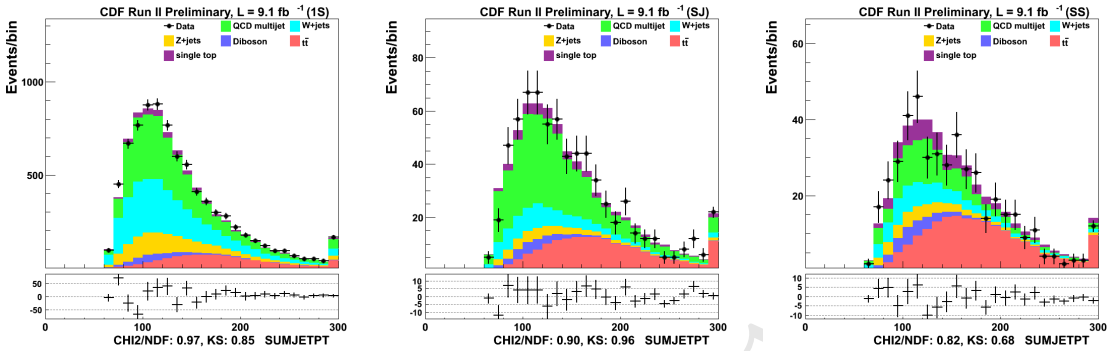

Figure 69: SUMJETPT stack plots in 1S, SJ, SS regions

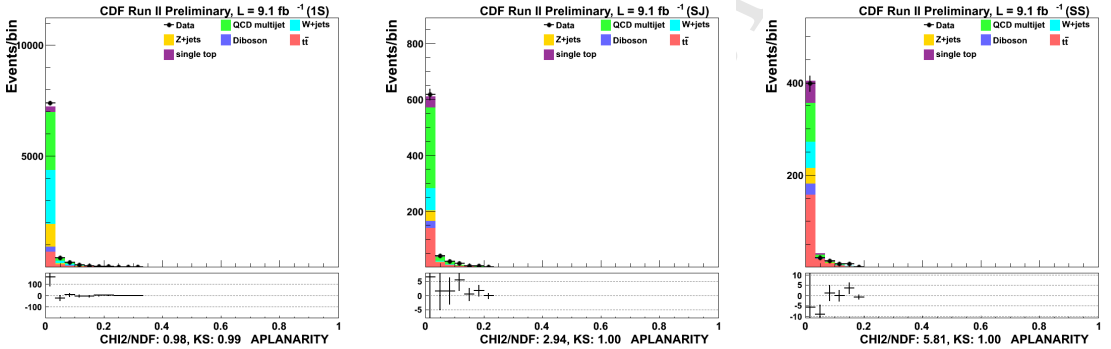

Figure 70: APLANARITY stack plots in 1S, SJ, SS regions

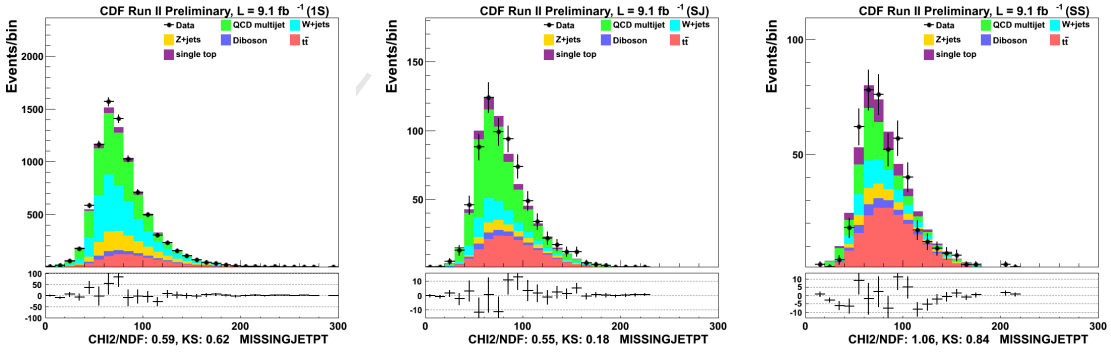

Figure 71: MISSINGJETPT stack plots in 1S, SJ, SS regions

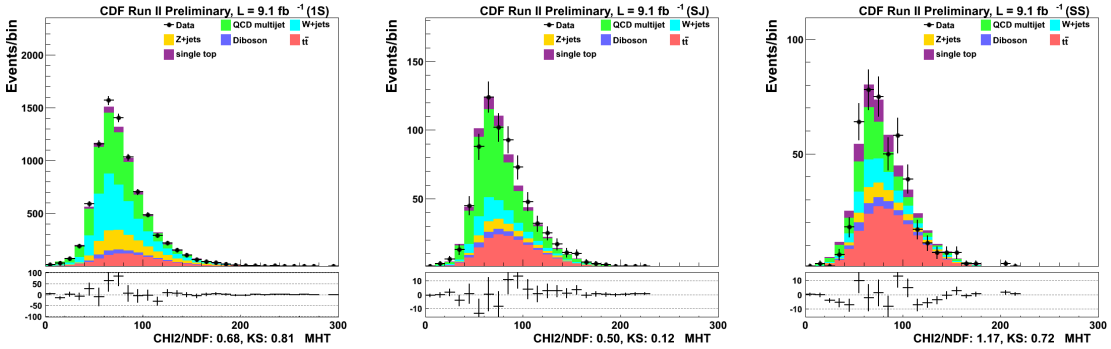

Figure 72: MHT stack plots in 1S, SJ, SS regions

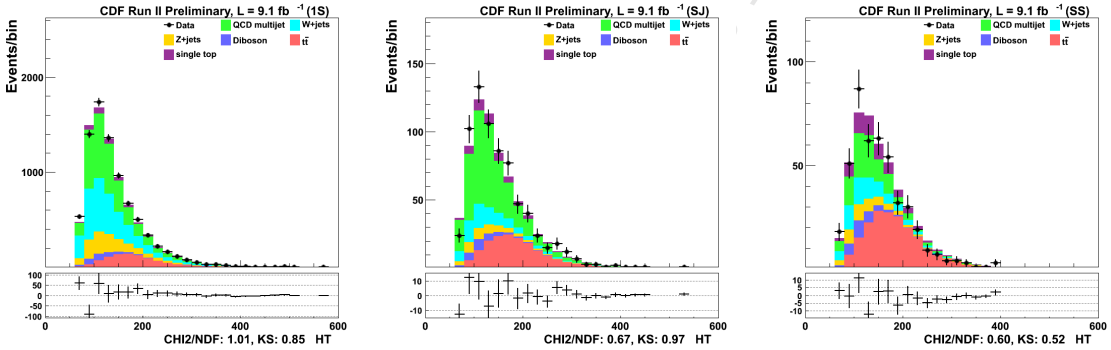

Figure 73: HT stack plots in 1S, SJ, SS regions

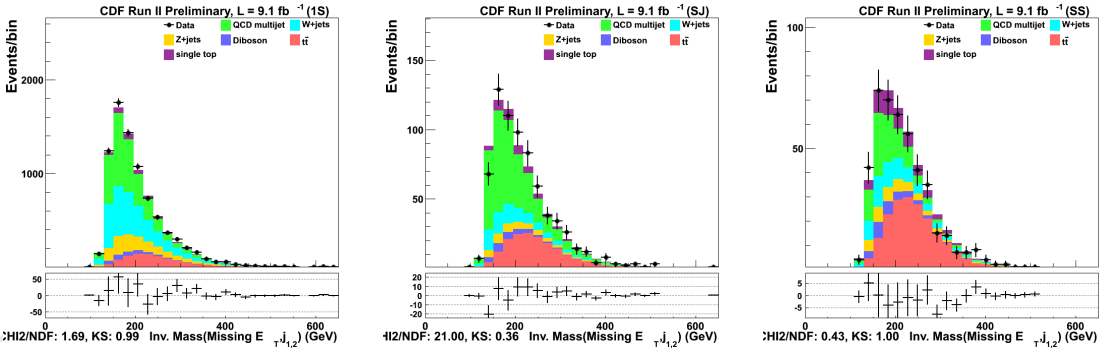

Figure 74: MVJ12 stack plots in 1S, SJ, SS regions

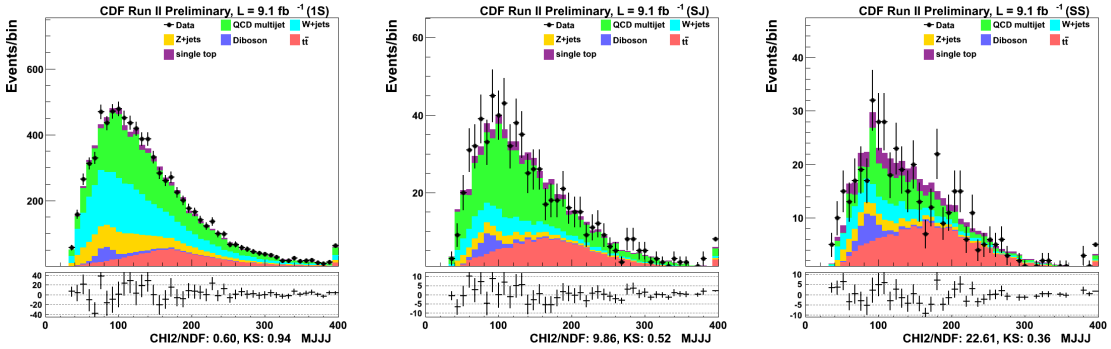

Figure 75: MJJJ stack plots in 1S, SJ, SS regions

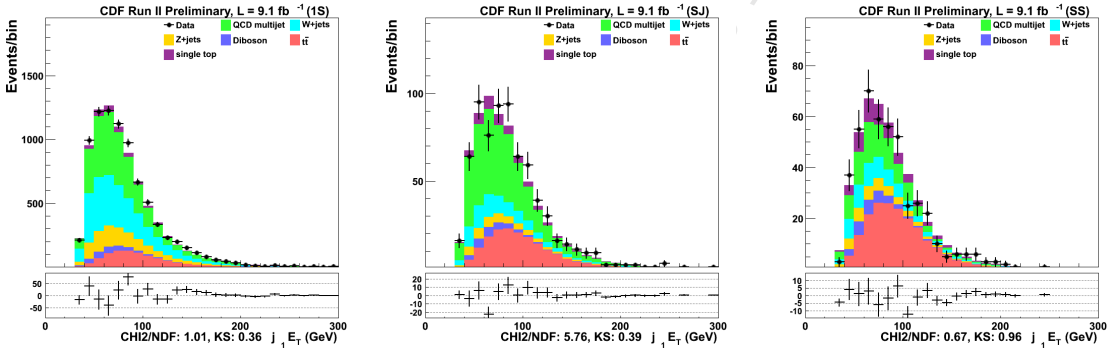

Figure 76: J1Et stack plots in 1S, SJ, SS regions

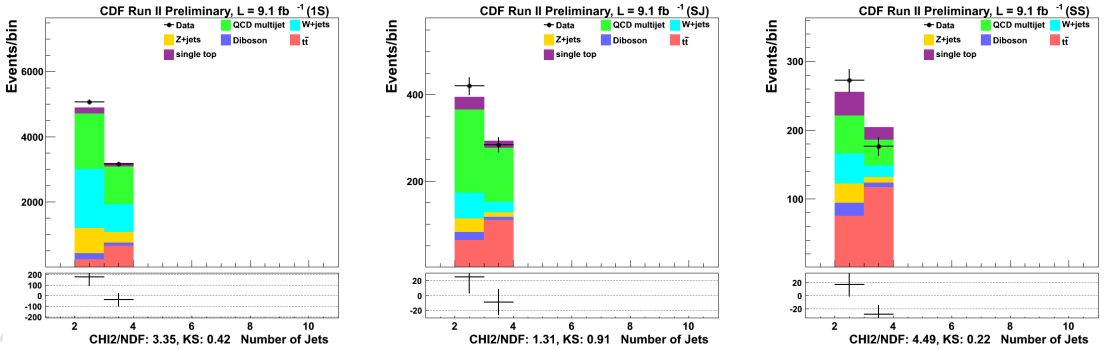

Figure 77: NJETS stack plots in 1S, SJ, SS regions

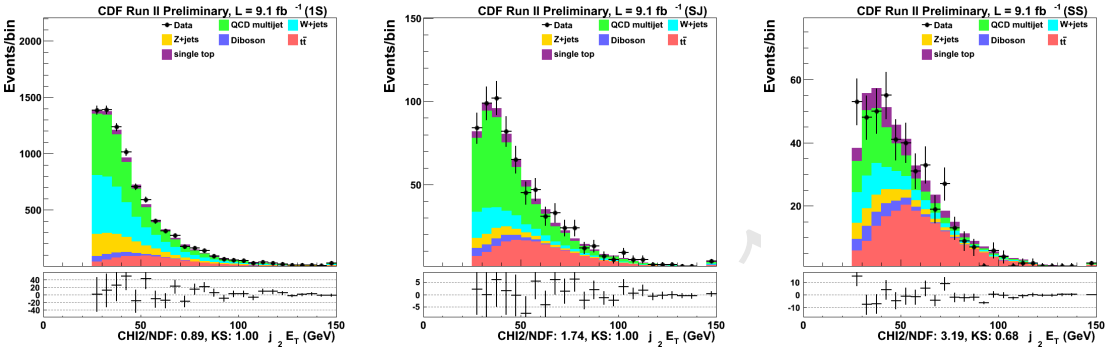

Figure 78: J2Et stack plots in 1S, SJ, SS regions

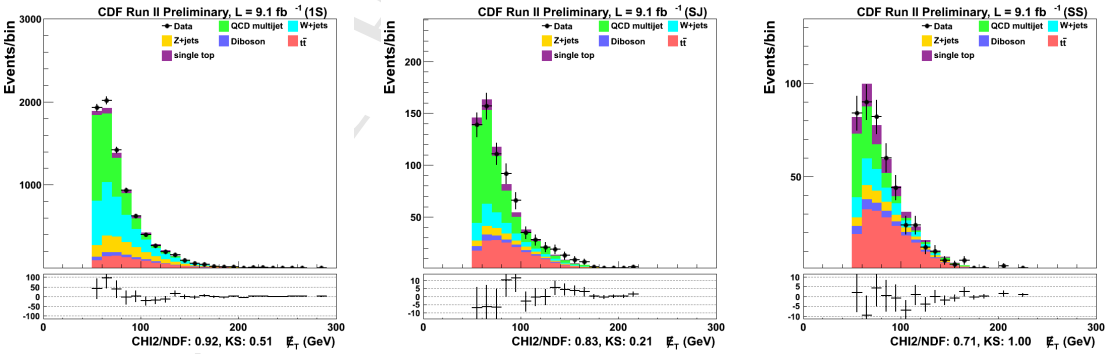

Figure 79: MET stack plots in 1S, SJ, SS regions

D SIGNN input variables

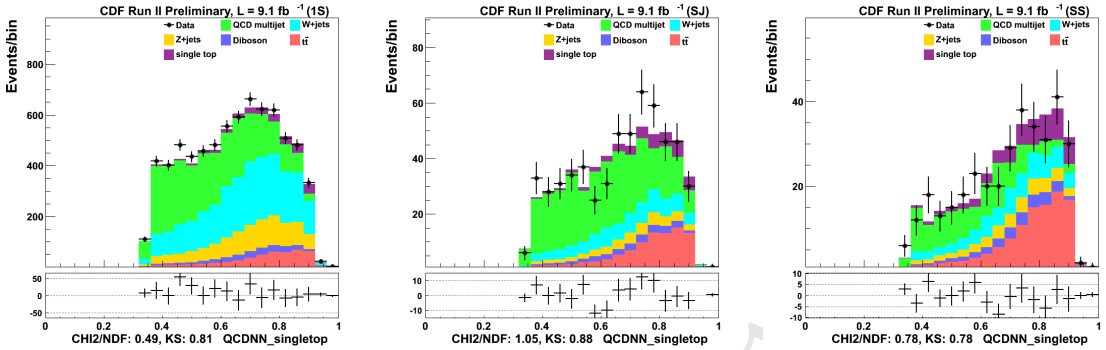

Figure 80: QCDNN.singletop stack plots in 1S, SJ, SS regions

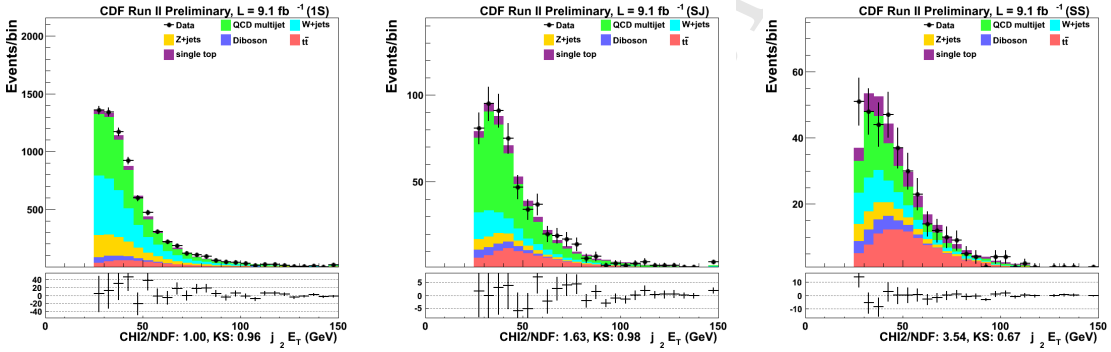

Figure 81: J2Et stack plots in 1S, SJ, SS regions

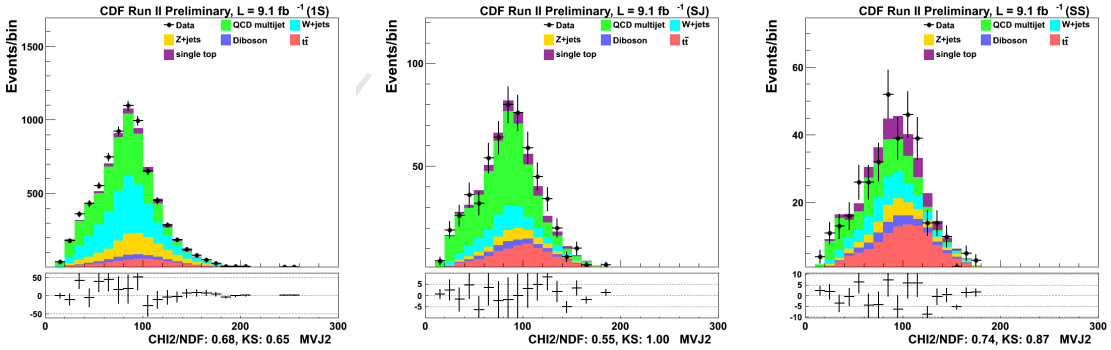

Figure 82: MVJ2 stack plots in 1S, SJ, SS regions

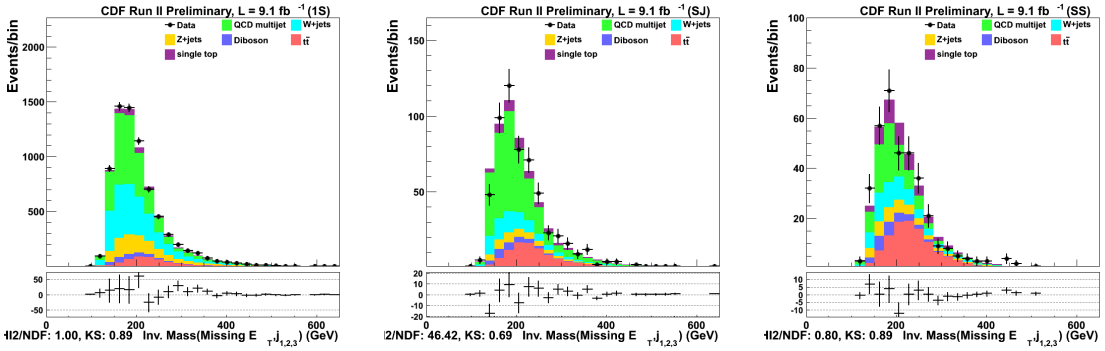

Figure 83: MVJ123 stack plots in 1S, SJ, SS regions

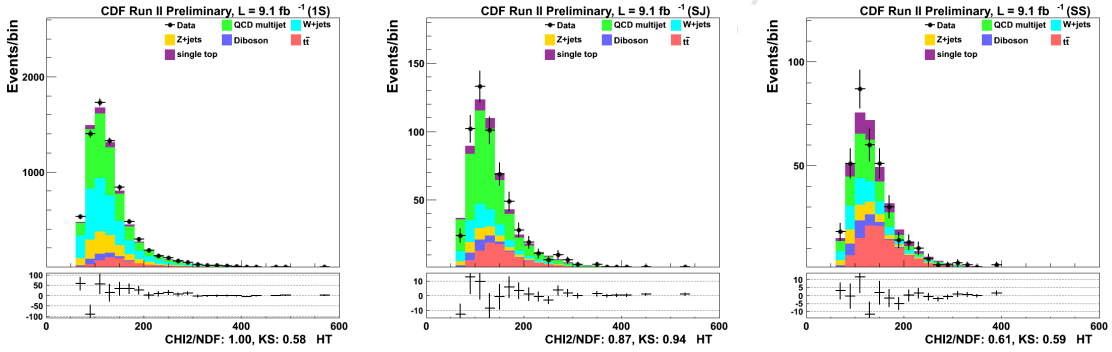

Figure 84: HT stack plots in 1S, SJ, SS regions

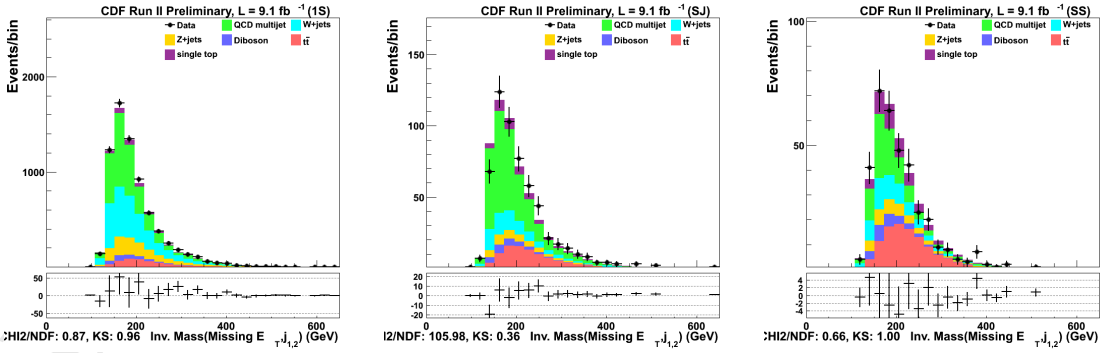

Figure 85: MVJ12 stack plots in 1S, SJ, SS regions

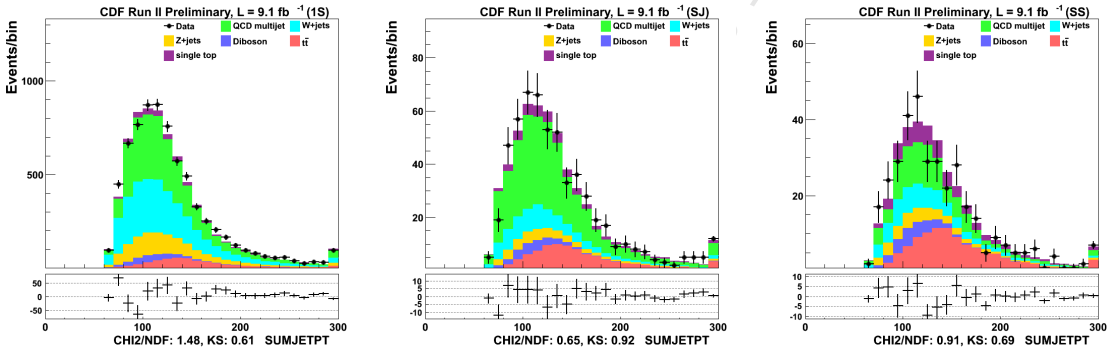

Figure 86: SUMJETPT stack plots in 1S, SJ, SS regions

References

[1] D.Abe et al. The CDF collaboration, Phys.Rev.Lett.74, 2626 (1995).

[2] S.Abachi et al. The D0 collaboration, Phys.Rev.Lett.74,2632 (1995).

[3] T. Aaltonen et al. First Observation of Electroweak Single Top Quark Production, Phys. Rev. Lett., 103:092002, 2009.

[4] V. M. Abazov and Abbott et al. Observation of single top-quark production. Phys. Rev. Lett., 103(9):092001, Aug 2009.

[5] Johan Alwall et al. Is V(tb) = 1? Eur. Phys. J., C49:791801, 2007.

[6] Gregory Mahlon and Stephen J. Parke. Improved spin basis for angular correlation studies in single top quark production at the Tevatron. Phys. Rev., D55:72497254, 1997.

[7] Gregory Mahlon and Stephen J. Parke. Single top quark production at the LHC: Understanding spin. Phys. Lett., B476:323330, 2000.

[8] Harris, B. W. and Laenen, E. and Phaf, L. and Sullivan, Z. andWeinzierl, S., Fully differential single-top-quark cross section in next-to-leading order QCD, Phys. Rev. D, 66, 054024, 2002

[9] Sullivan, Zack, Understanding single-top-quark production and jets at hadron colliders, Phys. Rev. D, 70, 114012, 2004

[10] Nikolaos Kidonakis, Single top quark production at the Fermilab Tevatron: Threshold re- summation and finite-order soft gluon corrections, Phys. Rev. D, 74, 114012, 2006

[11] Giorgio Bellettini, Matteo Cremonesi, Giuseppe Latino, Vadim Rusu, Marco Trovato, George Velev, Caterina Vernieri, Development of a tt veto in the search for WZ/ZZ production in events with lepton(s) plus jets plus missing transverse energy, CDFNOTE 10838

[12] A. Apresyan, D. Bortoletto, F. Margaroli, K. Potamianos, Oscar Gonzalez, M.Vidal, Song Ming Wang, Event selection for Higgs search in the $\not\!\!E_T$ plus jets sample, CDF 9358, 2008

[13] A.Mehta, Calibration of H1 Algorithm Improved Jets, CDF/DOC/CDF/GROUP/8564, 2006

[14] Qiuguang Liu, Karolos Potamianos, Fabrizio Margaroli, Daniela Bortoletto, Background Estimation in MET + b-Jets Analysis, CDFNOTE number 10452

[15] Daniela Bortoletto, Qiuguang Liu, Fabrizio Margaroli, Karolos Potamianos, Background Estimation in $\not\!\!E_T$ + b-jets Analysis, CDF/ANAL/MISSING ET/CDFR/10452

[16] Evelyn Thomson et. al Combination of CDF and D0 ttbar cross-sections, CDF note 10916

[17] J. Adelman et al., Method II For You, CDF Internal Note 9185, 2008.

[18] Frankiln, et al., Calibration of Heavy-Flavor Production in QCD Data, CDF NOTE 8768
Frankiln, et al., Heavy-Flavor Content of the W+Jets Sample, CDF NOTE 8765

[19] S. Jindariani, S. Klimenko, J. Konigsberg, G. Lungu, V. Necula, L. Pinera, A. Pronko, R. Rossin, A. Sukhanov, D. Tsybychev, S.M. Wang, Luminosity Uncertainty for Run 2 up until August 2004, CDF/ANAL/CDF/7446

[20] Oscar Gonzalez, Carsten Rott, Uncertainties due to the PDFs for the gluino-sbottom search, CDF/PHYS/EXOTIC/CDFR/7051

[21] C. Rott, at al. CDF Note 7136, Search for Scalar Bottom Quarks from Gluino Decays in Proton-Antiproton Collisions at 1.96TeV, PhD Thesis, CDF/THESIS/EXOTIC/PUBLIC/7526, 2005.

[22] Sensitivity, Exclusion and Discovery with Small Signals, Large Backgrounds, and Large Systematic Uncertainties, CDF note CDF/DOC/STATISTICS/PUBLIC/8128 (2007)

[23] M. L. Mangano et al, ALPGEN, a generator for hard multiparton processes in hadronic collisions, J. High Energy Phys. 0307 (2003) 001

[24] O. Gonzalez and M. Vidal, Getting ready for the 4 fb-1 dataset: Trigger efficiency of the MET+JETS samples, CDF/PHYS/MISSING_ET/CDFR/9745